haematologica
Journal of the Ferrata Storti Foundation

Characterization of tumor microenvironment and cell interaction patterns in testicular and diffuse large B-cell lymphomas

by Matias Autio, Oscar Brück , Marjukka Pollari, Marja-Liisa Karjalainen-Lindsberg, Klaus Beiske, Judit Mészaros Jørgensen, Harald Holte, Teijo Pellinen, Suvi-Katri Leivonen, and Sirpa Leppä

Received: July 12, 2024.
Accepted: December 2, 2024.

Citation: Matias Autio, Oscar Brück , Marjukka Pollari, Marja-Liisa Karjalainen-Lindsberg, Klaus Beiske, Judit Mészaros Jørgensen, Harald Holte, Teijo Pellinen, Suvi-Katri Leivonen, and Sirpa Leppä. Characterization of tumor microenvironment and cell interaction patterns in testicular and diffuse large B-cell lymphomas.
Haematologica. 2024 Dec 12. doi: 10.3324/haematol.2024.286267 [Epub ahead of print]

Characterization of tumor microenvironment and cell interaction patterns in testicular and diffuse large B-cell lymphomas

Matias Autio[1,2,3], Oscar Brück[4,5], Marjukka Pollari[1,3,6], Marja-Liisa Karjalainen-Lindsberg[7], Klaus Beiske[8], Judit Mészaros Jørgensen[9], Harald Holte[10], Teijo Pellinen[11], Suvi-Katri Leivonen[1,2,3], and Sirpa Leppä[1,2,3]

[1]Research Programs Unit, Applied Tumor Genomics, University of Helsinki, Helsinki, Finland
[2]Department of Oncology, University of Helsinki and Helsinki University Hospital Comprehensive Cancer Center, Helsinki, Finland
[3]iCAN Digital Precision Medicine Flagship, Helsinki, Finland
[4]Hematoscope Lab, Comprehensive Cancer Center & Center of Diagnostics, Helsinki University Hospital, Helsinki, Finland
[5]Department of Oncology, University of Helsinki, Helsinki, Finland
[6]Department of Oncology, Tampere University Hospital, Tampere, Finland
[7]Department of Pathology, Helsinki University Hospital, Helsinki, Finland
[8]Department of Pathology, Oslo University Hospital, Oslo, Norway
[9]Department of Hematology, Aarhus University Hospital, Aarhus, Denmark
[10]Department of Oncology, and KG Jebsen Centre for B cell malignancies, Oslo University Hospital, Oslo, Norway
[11]Institute for Molecular Medicine Finland (FIMM), Helsinki, Finland

Corresponding author:
Sirpa Leppä, MD, Professor
Department of Oncology and Research Programs Unit
University of Helsinki and Helsinki University Hospital Comprehensive Cancer Center
P.O. Box 180
FI-00029 Helsinki
Finland
Phone: +358 407558293
e-mail: sirpa.leppa@helsinki.fi

Short Title: DLBCL microenvironment organization and survival

Trial registration
Trials were registered at clinicaltrials.gov (NCT01502982 and NCT01325194).

Data availability statement
Data are available from the corresponding author upon reasonable request.

Acknowledgments
We thank Annabrita Schoonenberg (FIMM) and the Digital and Molecular Pathology Unit supported by Helsinki University and Biocenter Finland for performing the mIHC stainings, Anne Aarnio for technical assistance, and biorender.com for support in designing the visual abstract.

Funding
This research was funded by grants from the Research Council of Finland (S.L.), Finnish Cancer Organizations (S.L.), Sigrid Juselius Foundation (S.L.), University of Helsinki (S.L.), Helsinki University Hospital (S.L.), iCAN Digital Precision Cancer Medicine Flagship (S.L.), Biomedicum Helsinki Foundation (M.A.), Finnish Society of Oncology (M.A.), Finska Läkaresällskapet (M.A.), the Finnish Medical Foundation (M.P.), the Maud Kuistila Memorial Foundation (M.P.), and the Relander Foundation (M.P.).

Authorship Contributions
M.A. and S.-K.L. designed and conceived the study, analyzed data, and wrote the manuscript. O.B. performed cell interaction analyses. M.P. designed the study and participated in data analysis. M.-L.K.-L., K.B., J.M.J., and H.H. provided samples. T.P. designed and performed mIHC data analyses. S.L. designed and supervised the study and wrote the manuscript. All authors revised and accepted the final manuscript.

Disclosure of Conflicts of Interest
O.B. declares the following competing financial interests: Consultancy fees from Novartis, Sanofi, GSK, Astellas, and Amgen, outside the submitted work; research grants from Pfizer and Gilead Sciences, outside the submitted work; stock ownership of Hematoscope Ltd, outside the submitted work.

M. P. declares the following competing financial interests: Consultancy fees from Abbvie, Gilead, Roche, and Sobi, all outside the submitted work; honoraria from Abbvie, Astra Zeneca, and Gilead. H.H. declares the following competing financial interests: Honoraria, Advisory board for Incyte, Serbe, H, inoraria, Safety committee for Genmab, Nordic Nanovector, all outside the submitted work.

J.M.J. declares the following financial interest, not related to this work: consultancy for Abbvie, Gilead, Roche, Celgene/BMS, Incyte, SOBI, Novartis, Orion.

S.L. declares the following competing financial interests: Consultancy fees from Abbvie, Genmab, Gilead, Incyte, Novartis, Roche, and Sobi, all outside the submitted work; honoraria from Gilead, Incyte, Novartis, and Sobi; research grants from Bayer, Celgene/BMS, Hutchmed, Genmab, Novartis, and Roche, all outside the submitted work.

Abstract

The tumor microenvironments (TME) of diffuse large B-cell lymphoma (DLBCL) subgroups have remained poorly characterized. Here, we dissected the composition and spatial organization of the TME in germinal center B-cell (GCB), activated B-cell (ABC), and testicular DLBCLs (T-DLBCL) using gene expression profiling and multiplex immunohistochemistry. We found that high proportions of M2-like tumor-associated macrophages (TAMs) and cytotoxic tumor-infiltrating T cells (TILs) were characteristic of ABC DLBCL TME. Furthermore, high $CD8^+$ TIL content translated to favorable outcomes. In contrast, GCB DLBCL TME was enriched in $CD4^+$ TILs, regulatory TILs, and a higher M1-like/M2-like TAM ratio, and high proportions of TAMs and Granzyme B^+ cells associated with worse survival. TILs and TAMs interacted more frequently with M2-like TAMs and cytotoxic TILs in the ABC DLBCLs contrary to GCB subtype, where the interactions were more abundant with other TILs and $CD4^+$ TILs. In T-DLBCL, TME resembled that of ABC DLBCL with a higher proportion of M2-like TAMs and cytotoxic cells, except that checkpoint-positive TILs were less prominent compared to DLBCL NOS. Cytotoxic TILs also interacted more with TILs and TAMs. A high amount of $CD163^+$ TAM interactions with distinct TILs translated to unfavorable survival both in GCB DLBCL and T-DLBCL, whereas a high number of interactions between TILs and TAMs, $CD4^+$ TILs and TAMs, and $CD4^+$ TILs and other TILs associated with favorable outcomes only in T-DLBCL. Together, our data demonstrate biologically and clinically relevant differences in the composition of and cellular interactions in the TME between various DLBCL entities.

Introduction

The tumor microenvironment (TME) of diffuse large B-cell lymphoma, not otherwise specified (DLBCL, NOS), is heterogeneous. It consists of blood vessels, extracellular matrix, stromal cells, and variable proportions of immune cells, including T lymphocytes, macrophages, and NK cells reacting to the emergence of pathogenic lymphocytes[1, 2]. However, TME can also promote lymphoma growth by offering pro-tumorigenic signals and a protective milieu to lymphoma cells[3]. Based on gene expression profiles reflecting differences in the composition of the TME, novel DLBCL subtypes with distinct biological features and outcomes have recently been proposed[4, 5]. Likewise, clinical associations of distinct tumor infiltrating immune cell phenotypes, including checkpoint molecule-expressing T lymphocytes and macrophages have also been discovered and the spatial organization of the TME has also been uncovered[6-14]. To date, however, different TME-targeted therapies, such as PD-1 blockade have not shown any clinically significant efficacy in DLBCL, and further characterization of factors predictive for outcome is warranted[15].

Based on the cell-of-origin (COO), DLBCL NOS (DLBCL) is divided into germinal center B-cell (GCB) and activated B-cell (ABC) -like molecular subtypes[16]. The subtypes differ clinically, with GCB DLBCLs having a higher sensitivity to first-line treatment consisting of rituximab, cyclophosphamide, doxorubicin, vincristine, and prednisone (R-CHOP)[17, 18]. Biologically, they harbor different genetic aberrations reflecting different pathogenesis[19, 20]. While GCB DLBCL originates from GCB cells with frequent alterations in genes, such as *BCL2* and *EZH2*, ABC DLBCL is derived from more mature, post-GC B cells, and it is characterized by continual activity of the NF-κB pathway[21-23]. Based on genetic aberrations DLBCL can also be divided into distinct genetic subgroups[24, 25].

Testicular diffuse large B-cell lymphoma (T-DLBCL) is a rare lymphoid malignancy of the testes, most commonly arising among elderly males[26]. Most cases represent ABC DLBCL molecularly, and in the advanced stage, they are at high risk of recurrence and have a dismal prognosis[27].

We have previously shown that based on the TME composition, DLBCL can be classified into inflamed and non-inflamed subtypes[11, 12]. While the inflamed subtype is associated with favorable outcome in T-DLBCL[28], immune checkpoint expression in T cells and low T cell/macrophage proportion translates to inferior outcome in DLBCL NOS[11, 12]. Despite the evidence of its clinical significance, differences in the composition and spatial organization of the TME between GCB, ABC, and T-DLBCLs have been poorly characterized. We hypothesized that the differences in the pathogenesis, biology, and clinical outcome of these subtypes are reflected in the TME. Here, we compare the TME composition and cell interaction patterns between these subtypes, and how they associate with survival.

Methods

Patients and samples

Study populations are presented in Table S1. DLBCL gene expression cohort consisted of 69 patients treated in the Nordic LBC-05 and LBC-04 trials[29, 30], whereas T-DLBCL gene expression, DLBCL multiplex immunohistochemistry (mIHC), and T-DLBCL mIHC cohorts consisted of 60, 175 and 80 retrospectively collected patients, respectively. Thirty-four DLBCL patients and 60 T-DLBCL patients were overlapping between the gene expression and mIHC cohorts. Patients with high-grade B-cell lymphoma were excluded. We constructed tumor microarrays (TMAs) from formalin-fixed paraffin-embedded (FFPE) primary diagnostic tumor tissue[31]. We also used gene expression data of 496 DLBCL patients from the Reddy et al. (EGAS00001002606) and 562 DLBCL patients from the Schmitz et al. cohorts[24, 32].

The study was approved by the Ethics Committee of Helsinki University Hospital, Finland, the Finnish National Authority for Medicolegal Affairs (VALVIRA), and the Institutional Review Board. The patients treated in Nordic phase II studies LBC-04 and LBC-05 signed an informed consent before study enrollment. Sample collection was performed following the Declaration of Helsinki.

Gene expression profiling

We used Nanostring gene expression data performed on primary diagnostic FFPE tumor tissue using a Nanostring nCounter Human PanCancer Immunoprofiling Panel (XT-CSO-HIP1-12, Nanostring Technologies, Seattle, WA)[11, 28]. Molecular subtypes determined with DLBCL90 assay (NanoString) were available for 47/69 patients (68%) in the DLBCL gene expression cohort. For the DLBCL mIHC cohort, COO was available for 137 patients (78%) based on RNA sequencing (n=101) and Lymph2Cx assay (n=36)[33, 34].

Immunohistochemistry and cell-to-cell interaction analyses

We used mIHC data performed on TMAs constructed from diagnostic FFPE tumor tissue of 175 patients with primary DLBCL and 80 patients with primary T-DLBCL[11, 12, 35]. We characterized T cells, macrophages, NK cells, B cells, and immune checkpoint molecules (Table S2). All mIHC panels are described in detail in Supplementary Methods. We filtered out areas with staining artifacts using Ilastik v.1.3.3 software and performed automated digital quantification using CellProfiler v.3.1.8 software (https://cellprofiler.org/)[36, 37]. We had previously performed IHC stainings for β_2 microglobulin (B2M), HLA-ABC, and HLA-DR[11, 28].

Cell-to-cell interaction analyses were performed on 229 mIHC stained samples, using the method developed by Brück et al[38]. We defined cells with a Euclidean distance < 100 pixels (22µm) from each other as interacting cells[39]. We calculated an interaction index based on the number of cell-to-cell interactions normalized to the number of corresponding cell types in each sample. More details are provided in the Supplementary Methods.

Statistical analyses

We performed all statistical analyses using R v.4.1.2. For unsupervised hierarchical clustering analyses we used Euclidean distance and Ward's linkage. We used univariable and multivariable

Cox proportional hazards regression models to estimate the prognostic significance of each variable, and the Kaplan-Meier method with log-rank test to estimate the difference in survival between patient groups. We defined overall survival (OS) as the time from diagnosis to death from any cause and progression free survival (PFS) as the time from diagnosis to progression or death from any cause. We used Mann-Whitney U and Kruskal-Wallis H tests to compare two or more groups, respectively. The Benjamini-Hochberg method was used to correct P-values for errors caused by multiple testing.

Results

Patient characteristics

Patient characteristics of the five study cohorts are presented in Table S1. The *DLBCL gene expression cohort* consisted of 69 patients. Median age was 55 years (range 22-65), and disease characteristics were typical of high-risk DLBCL[11]. Median follow-up time was 65 months (interquartile range (IQR): [51 months;68 months]), during which 11 patients relapsed and 9 died translating to 86% and 88% 5-year PFS and OS rates. Twenty-four (35%) patients had GCB DLBCL, 16 (23%) had ABC DLBCL, and 7 (10%) remained unclassified. In 22 (32%) cases, data on the COO was unavailable. Five-year OS rates for the patients with GCB and ABC DLBCL were 95.8% and 87.5%, (p=0.300), respectively.

The *DLBCL mIHC cohort* consisted of 175 patients with a median age of 61 years (range 16-84). During a median follow-up time of 62 months (IQR: [44 months;68 months]), 28 patients relapsed and 33 died translating to 76% PFS and 79% OS at 5 years[12]. Sixty-one (35%) patients had GCB DLBCL, 58 (33%) had ABC DLBCL, and 18 (10%) were unclassified. In 38 (22%) cases, data on COO was unavailable. Five-year OS rates for the patients with GCB DLBCL and ABC DLBCL were 92.9% and 64.6% (p<0.001), respectively.

The *T-DLBCL gene expression* and *mIHC cohorts* consisted of 60 and 80 patients, with median ages of 69 years (range 36-83) and 70 years (range 36-92)[28, 35]. As typical for T-DLBCL, most patients (40/60 (67%) in the gene expression cohort and 56/80 (70%) in the mIHC cohort) had non-GC DLBCL. In the gene expression cohort, the median follow-up time was 76 months (IQR: [54 months;134 months]), during which 27 patients relapsed or died and in the mIHC cohort 76 months (IQR: [53 months;133 months]), during which 41 patients relapsed or died. Five-year OS rates were 60.1% in the gene expression cohort and 53.6% in the mIHC cohort.

Expression of immune-related genes in the GCB and ABC DLBCLs

To get an overview of the immunological landscape of GCB and ABC DLBCLs, we first analyzed the differential expression of immune-related genes using a Nanostring nCounter platform. As expected, ABC DLBCLs expressed high levels of ABC markers, such as *TNFRSF13B* and *IRF4* but also genes related to macrophage signaling, such as *CD163* and *CD47*. In comparison, GCB DLBCLs overexpressed genes related to T-cell receptor signaling, such as *ICOSLG*, *HLA-DOB*, *IL4*, and *CD40LG* (Figure 1A and Table S3). Furthermore, using unsupervised hierarchical clustering, we could accurately separate GCB and ABC subtypes based on the expression of these most differentially expressed immune-related genes (adj. p<0.01) (Figure 1B).

To validate our findings, we used RNA-seq data from 496 DLBCLs from the Reddy et al. cohort and 562 DLBCLs from the Schmitz et al. cohort[24, 32]. By analyzing the same gene set as in the Nanostring cohort, we found that many of the previously identified genes were differentially expressed also in the validation cohorts (Figure S1A and S2A and Table S4). Analogously, clustering of the most differentially expressed immune-related genes separated GCB and ABC subtypes (Figure S1B and S2B). Likewise, genes associated with macrophage signaling, such as *CD163*, and cytotoxicity, such as GZMB, GZMH, GZMM, and PRF1, were overexpressed in the ABC subtype in the Reddy et al. cohort (adj. p<0.001 for all; Figure S1C-P). Instead, we did not

observe any significant differences in the expression of *CD3*, *CD4*, or *CD8* T cell genes (Figure S1H-L).

The composition of the TME differs between GCB and ABC DLBCL

Next, we studied the composition of the TME at the cellular level using mIHC in 175 DLBCL NOS samples (Figure 2A). Comparing the TME compositions between GCB and ABC subtypes, we found that $CD163^+$ tumor-associated macrophages (TAMs) were enriched in the ABC subtype (median; 11.9% vs. 3.84%, adj. $p<0.001$), whereas in the GCB subtype, a higher proportion of all TAMs were CD163 negative (median; 79.2% vs. 52.0%, adj. $p<0.001$) (Figure 2B-D and Table S5). When we analyzed tumor-infiltrating T lymphocytes (TILs), we did not observe significant differences in the proportion of TILs as such between the two molecular subtypes (median; ABC; 14.5% vs. GCB; 13.9%, adj. $p=0.448$) (Figure S3A-C). However, in the GCB subtype, a higher proportion of TILs were $CD4^+$ T helper cells (median; 66.1% vs. 55.8%, adj. $p=0.023$) and regulatory T cells (Tregs) (median; 8.66% vs. 5.26%, adj. $p=0.015$), whereas in the ABC subtype, a higher proportion of TILs were Granzyme B^+ (GrB^+) (median; 1.02% vs. 0.39%, adj. $p=0.008$) (Figure 2E-G). In addition, GrB^+ cytotoxic cells as such were more abundant in the ABC subtype (median; 0.38% vs. 0.14%, adj. $p=0.002$) (Figure S3D). Interestingly, the proportion of immune checkpoint-expressing cells also differed according to the subtype, PD-$L1^+$ $CD163^+$ TAMs being more frequent in ABC DLBCL (median; 0.74% vs. 0.10%, adj. $p=0.001$) (Figure 2H and Figure S3E-I). Finally, the presence of immune cells altogether tended to be higher in the TME of ABC DLBCL, as analyzed by the amount of CD20 negative cells, although statistical significance was not reached (median; 42.2% vs. 35.0%, adj. $p=0.065$) (Figure S3J).

Next, we sought to uncover, whether the expression of HLA and B2M differ between GCB and ABC DLBCLs. We observed higher expression of HLA-ABC and B2M in the ABC subtype compared to the GCB subtype (HLA-ABC^+; 67% vs. 32%, $p<0.001$; $B2M^+$; 37% vs. 12%, $p=0.005$). However, there was no difference in the HLA-DR positivity between the subtypes ($p=0.835$) (Figure

S3K). Furthermore, neither the proportion of HLA-ABC nor B2M correlated with the proportion of TILs or TAMs (Figure S4).

The TME of T-DLBCL compared to DLBCL, NOS

We wanted to extend our analyses to T-DLBCLs, which typically are of ABC origin, and to uncover whether T-DLBCLs resembled ABC DLBCL in their TME composition. However, in a principal component analysis (PCA) based on the expression of immune-related genes in 60 T-DLBCL and 69 DLBCL NOS samples, T-DLBCLs were separated from the DLBCL samples (Figure 3A). Similarly, in an unsupervised hierarchical clustering including all immune-related genes, T-DLBCLs and DLBCL cases formed separate clusters, except for one ABC DLBCL, which clustered with T-DLBCLs (Figure S5A). Especially genes related to cell division, such as *CDK1*, *BIRC5*, and *PRKCE*, and genes related to B-cell receptor signaling, such as *BCL2*, *CD79B*, *NFKB1*, and *BLNK* were upregulated whereas genes related to antigen presentation and processing and T-cell activation, including many HLA genes, were downregulated in T-DLBCL compared to DLBCL (Figure S5B and Table S6). The results show that clinical subtype is a stronger determinant of the TME composition than COO.

Considering the significance of the clinical subtype on the expression of immune-related genes, we then compared 80 T-DLBCL samples with 175 DLBCL samples analyzed by mIHC to reveal potential differences in the composition of the TME between T-DLBCL and DLBCL on the cellular level (Figure S5C and Table S7). Compared to DLBCL, the TME of T-DLBCL consisted of a higher proportion of GrB^+ cytotoxic cells and $CD163^+$ TAMs (median; 0.70% vs. 0.20%, adj. $p<0.001$ and 12.4% vs. 6.21%, adj. $p=0.001$, respectively) in particular, whereas the proportion of TILs altogether, T helper cells, Tregs and $CD163^-$ TAMs was significantly lower (median; 9.78% vs. 14.5%, adj. $p=0.009$, 5.94% vs. 9.79%, adj. $p<0.001$, 0.24% vs. 0.85%, adj. $p<0.001$ and 3.59% vs. 5.84%, adj. $p<0.001$, respectively) (Figure S6A-I). We also observed that the proportion of different $PD\text{-}1^+$ cells and $LAG3^+$ lymphocytes was lower in T-DLBCL compared to DLBCL ($PD\text{-}1^+$ cells median; 3.97% vs. 6.26%, adj. $p=0.015$) (Figure S6J-L). To investigate whether the

differences in the composition of the TME between T-DLBCL and DLBCL result from the fact that most T-DLBCLs are of ABC origin, we compared the TME composition of GCB and ABC DLBCL separately with GC and non-GC type T-DLBCL. We found only minor differences between the TMEs of GC and non-GC T-DLBCL (Figure 3B-E and Figure S6M-U). The proportion of some cell types, such as GrB+ cells and $CD163^+$ TAMs in GC and non-GC T-DLBCL were comparable with ABC DLBCL, whereas the proportion of other cell types, such as $CD163^-$ TAMs and Tregs were lower in T-DLBCL compared to both GCB and ABC DLBCL (Figure 3B-E and Figure S6M-U). Taken together, the TMEs of these lymphomas seem to represent a continuum with GCB DLBCL at one end, and non-GC T-DLBCL at the other.

Lastly, we analyzed the expression of HLA molecules in T-DLBCLs compared to DLBCLs. Although the expression of HLA-ABC and B2M was significantly higher in ABC DLBCL compared to GCB DLBCL, the expression of HLA-ABC, HLA-DR, and B2M was less common in T-DLBCLs than in ABC DLBCLs (29% vs 67%, $p<0.001$, 17% vs 33%, $p=0.070$, and 13% vs 37%, $p=0.006$, respectively) and expression of HLA-ABC and B2M was comparable to GCB DLBCLs (29% vs 32%, $p=0.837$ and 13% vs 12%, $p=1.000$) (Figure 3F and Figure S6V).

Differences in cell-to-cell interaction patterns between GCB, ABC, and T-DLBCLs

Next, we wanted to find out, whether the differences in the TME composition between GCB and ABC DLBCLs were associated with spatial cell-to-cell interactions. When we compared TIL interactions overall, we found TILs in general and T helper cells in particular had more interactions with other TILs and TAMs (adj. $p<0.001$ for all) (Figure 4 and Figure S7A-B). In addition, B cells had more interactions with PD-$L1^+$ cells in the GCB subtype (Figure 4). On the contrary, cytotoxic TILs interacted more often with T helper cells, cytotoxic T cells, and TAMs in general (adj. $p<0.001$, adj. $p=0.003$, and adj. $p=0.017$) (Figure 4 and Figure S7A-B). We did not find any major differences in TAM interactions overall between the subtypes (Figure S7A-B). However, $CD163^+$ TAMs interacted more often with B cells, TILs, other TAMs, and PD-1^+ cells in the ABC DLBCLs compared to GCB DLBCLs (adj. $p<0.001$ for all) (Figure 4 and Figure S7A-B). Finally, we studied

the interactions of cells expressing immune checkpoint molecules. Notably, we found that PD-1$^+$ cells had more interactions with PD-L1$^+$ cells and more specifically PD-1$^+$ T helper cells and cytotoxic T cells had more interactions with PD-1$^+$ T helper cells in GCB DLBCL compared to ABC DLBCL (adj. p<0.001, adj. p=0.004, and adj. p=0.024) (Figure 4), whereas PD-L1$^+$ cells had more interactions with B cells in ABC DLBCL (adj. p=0.027) (Figure S7A-B).

In T-DLBCL, cell interactions resembled those in ABC DLBCL. However, there were some differences. Most notably, compared to ABC DLBCLs, in T-DLBCLs cytotoxic T cells had more interactions with other TME-associated cells, especially CD163$^+$ macrophages and PD-L1$^+$ cells (adj. p=0.015 and adj. p=0.005), but also with T helper cells and other cytotoxic T cells (adj. p=0.075 and adj. p=0.056). However, statistical significance was not retained after correction for multiple testing (Figure 4). In addition, B cells interacted more often with other B cells in T-DLBCLs compared to ABC DLBCLs (adj. p<0.001) (Figure 4).

Prognostic impact of immune cells and their interactions in the TME of GCB and ABC DLBCL

Beyond studying the differences in the composition of the TME, we investigated whether the impact of immune cell subtypes on survival differed between the ABC and GCB subtypes and T-DLBCL[28, 35, 40]. First, as we have previously reported in DLBCL NOS[12], the proportion of immune checkpoint-expressing TAMs, such as PD-L1 and TIM3 expressing CD163$^-$ TAMs associated with poor survival both in GCB and ABC DLBCL (PFS: GCB; HR=2.85, 95% CI 1.1-7.6, p=0.037, ABC; HR=2.92, 95% CI 1.0-8.1, p=0.041) (Figure 5A). In addition to immune checkpoint expressing TAMs, TAMs altogether, CD163$^+$ TAMs, and a higher proportion of PD-L1$^+$ cells, GrB$^+$ cytotoxic immune cells, and TIM3$^+$ TILs translated to adverse outcome in GCB but not in ABC DLBCL (PFS: HR=1.24, 95% CI 1.0-1.5, p=0.024, HR=1.24, 95% CI 1-06-2.14, p=0.021, HR=1.16, 95% CI 1.0-1.3, p=0.039, HR=1.51, 95% CI 1.1-2.1, p=0.021, and HR=1.23, 95% CI 1.0-1.4, p=0.010, respectively) (Figure 5A-D and Figure S8A-I). In contrast, a high proportion of CD8$^+$ TILs associated with better survival in patients with ABC DLBCL, but not in patients with GCB DLBCL

(PFS: ABC DLBCL; HR=0.92, 95% CI 0.84-1.0, *p*=0.048, GCB DLBCL; HR=1.01, 95% CI 0.89-1.1, *p*=0.888) (Figure 5A and Figure S8A and J-K).

Finally, we studied the prognostic impact of cell-to-cell interactions. Especially in GCB DLBCL, but also in T-DLBCL, a high amount of $CD163^+$ TAM interactions with TILs, T helper cells, and $PD\text{-}1^+$ cells translated to unfavorable survival (Figure 6A-B and Figure S9A-G). On the contrary, $CD163^+$ TAM interactions did not impact survival in patients with ABC DLBCL. In addition, in T-DLBCL, a high number of interactions between TILs and TAMs, T helper cells and TAMs, and T helper cells and other TILs associated with favorable outcomes (Figure 6A and C-D and Figure S9H-M).

Discussion

Previous studies have identified some differences in the TMEs between the GCB and ABC DLBCLs, such as greater cytotoxicity and increased expression of PD-L1 on B cells and macrophages in the ABC subtype[10, 41]. Additionally, certain differences in the spatial organization between the subtypes have been reported[13]. A comprehensive comparison of the TMEs between the GCB and ABC DLBCLs has, nevertheless, been missing. In this study, we dissected the composition and spatial organization of the TME in GCB and ABC DLBCLs, and T-DLBCL using gene expression profiling and mIHC. We found that ABC DLBCL typically has a more cytotoxic TME, and a predominance of M2-like TAMs, whereas the TME in GCB DLBCL is characterized especially by a larger proportion of T helper cells and Tregs. The TME in T-DLBCL is similar to the TME of ABC DLBCL, which is in line with the fact that T-DLBCL is usually of ABC origin. However, we also observed that the clinical subtype is a stronger determinant of the TME composition than COO. Our cell-to-cell interaction analyses indicated that the cell types overrepresented in each subtype are also more involved in the interactions with the other immune cells. Finally, we showed that the differences in the TME composition between the DLBCL subtypes further reflect the differences in the organization of their TMEs, with different cell types being clinically meaningful in distinct subtypes.

The TME of T-DLBCL resembled the TME of ABC DLBCL with higher proportions of cytotoxic immune cells and M2-like macrophages and fewer T helper cells. There were, however, also some differences, most notably the proportions of M1-like macrophages and Tregs. The total amount of B cells was also significantly lower in T-DLBCL compared to ABC DLBCL. However, the proportion of most immune cells in T-DLBCL was closer to the proportions in ABC DLBCL than to GCB DLBCL. Therefore, it seems that the ABC-type lymphomas shape their TME in T-DLBCLs in a similar manner as in ABC DLBCL. Nonetheless, the immune-privileged milieu of the testes most likely has its distinct and unique influence on the entire pathogenesis and the formation of the TME of T-DLBCL, differing somewhat from that of ABC DLBCL. All in all, it appears that in many cases, the TMEs in DLBCL and T-DLBCL represent a continuum with GCB DLBCL and T-DLBCL furthest away from each other and ABC DLBCL in the middle (Figure 7).

A possible explanation for the different compositions of the TME may be the expression of HLA molecules. We found higher expression of HLA-ABC and B2M in ABC compared to GCB DLBCL, being in line with earlier findings, where MHC-I loss was observed in both GC B cell (~60%) and ABC (~40%) molecular subtypes[42]. HLA-ABC molecules present fragments of proteins to cytotoxic cells, which might explain the accumulation of cytotoxic cells in the TME of ABC DLBCL. Previous studies have also found a correlation of HLA molecules with certain immune cell types of the DLBCL TME[28]. However, we did not find any direct association between the expression of HLA-ABC and the proportion of cytotoxic cells or any other major cell type in the TME. Another observation that contradicts the hypothesis of HLA molecules explaining the differences seen in the TME was the finding that T-DLBCL express less frequently HLA molecules than DLBCL NOS, although their TME is rich in cytotoxic cells. Therefore, the expression of HLA molecules is unlikely to be the principal reason behind the differences in the TMEs.

Previous studies have found multiple different immune cell subtypes correlating with the survival of DLBCL patients[7-12, 43, 44]. However, a comparison of the prognostic impact of these cell subtypes and especially their interactions in different DLBCL subtypes has been lacking. We found that the

prognostic impact of certain immune cells on survival differed between GCB and ABC DLBCL. Most notably, TAMs, PD-L1^{+} cells, GrB^{+} cells, and TIM3^{+} TILs associated with poor survival in GCB DLBCL, whereas, in addition to immune checkpoint expressing TAMs, only CD8^{+} TILs correlated positively with outcome in ABC DLBCL. Conversely, we have previously found that the total proportion of TILs, PD-L1^{+} TAMs, and PD-1^{+} TILs have a favorable, and TBET^{+}FOXP3^{+} Tregs an adverse impact on survival in patients with T-DLBCL[28, 35, 40]. The impact these cell types have on survival may be directly related to the different biology of the molecular subtypes. Despite the differences in biology and prognosis, treatment of GCB and ABC DLBCLs has remained the same, and TME-directed therapies have so far not been effective[15]. Our findings, nevertheless, raise the question of whether novel TME-targeted therapies could have different efficacy in GCB and ABC DLBCL, as well as in T-DLBCL.

The strengths of our study are multiple cohorts, the availability of both gene expression and immunohistochemical data, and the possibility to identify clinically relevant cell-cell interactions. The limitation is that we had only one mIHC cohort available to compare GCB and ABC subtypes. Although the results in two separate gene expression cohorts and ABC-dominated T-DLBCL cohorts further strengthened our observations, validation in a larger mIHC cohort is warranted. T-DLBCL patients were not uniformly treated, making validation of the prognostic impact of different immune cell subtypes and their interactions in this subtype in another cohort a necessity. Furthermore, data on which samples in the DLBCL NOS cohort were nodal and which extranodal was lacking. Finally, due to a limited number of samples with genetic information, there was insufficient statistical power to compare the genetic subtypes.

In summary, we have shown in multiple cohorts and overlapping methods that the TMEs of GCB and ABC DLBCLs are distinct. The TME in T-DLBCL resembles the TME of ABC DLBCL. However, clinical subtype is a stronger determinant of the TME composition than COO. Cell-to-cell interaction analyses indicate that the interplay between distinct tumor-infiltrating immune cells also differs according to the subtype. Finally, our data suggest that different TME-targeted therapies

might have distinct clinical efficacy based on the DLBCL subtype, although individual differences are undoubtedly also significant.

References

1. Scott DW, Gascoyne RD. The tumour microenvironment in B cell lymphomas. Nat Rev Cancer. 2014;14(8):517-534.
2. Nicholas NS, Apollonio B, Ramsay AG. Tumor microenvironment (TME)-driven immune suppression in B cell malignancy. Biochim Biophys Acta. 2016;1863(3):471-482.
3. Gajewski TF, Schreiber H, Fu YX. Innate and adaptive immune cells in the tumor microenvironment. Nat Immunol. 2013;14(10):1014-1022.
4. Kotlov N, Bagaev A, Revuelta MV, et al. Clinical and Biological Subtypes of B-cell Lymphoma Revealed by Microenvironmental Signatures. Cancer Discov. 2021;11(6):1468-1489.
5. Steen CB, Luca BA, Esfahani MS, et al. The landscape of tumor cell states and ecosystems in diffuse large B cell lymphoma. Cancer Cell. 2021;39(10):1422-1437.e10.
6. Fridman WH, Pages F, Sautes-Fridman C, Galon J. The immune contexture in human tumours: impact on clinical outcome. Nat Rev Cancer. 2012;12(4):298-306.
7. Cai QC, Liao H, Lin SX, et al. High expression of tumor-infiltrating macrophages correlates with poor prognosis in patients with diffuse large B-cell lymphoma. Med Oncol. 2012;29(4):2317-2322.
8. Keane C, Gill D, Vari F, Cross D, Griffiths L, Gandhi M. CD4(+) tumor infiltrating lymphocytes are prognostic and independent of R-IPI in patients with DLBCL receiving R-CHOP chemo-immunotherapy. Am J Hematol. 2013;88(4):273-276.
9. Riihijärvi S, Fiskvik I, Taskinen M, et al. Prognostic influence of macrophages in patients with diffuse large B-cell lymphoma: a correlative study from a Nordic phase II trial. Haematologica. 2015;100(2):238-245.
10. Xu-Monette ZY, Xiao M, Au Q, et al. Immune Profiling and Quantitative Analysis Decipher the Clinical Role of Immune-Checkpoint Expression in the Tumor Immune Microenvironment of DLBCL. Cancer Immunol Res. 2019;7(4):644-657.
11. Autio M, Leivonen SK, Brück O, et al. Immune cell constitution in the tumor microenvironment predicts the outcome in diffuse large B-cell lymphoma. Haematologica. 2021;106(3):718-729.
12. Autio M, Leivonen SK, Brück O, Karjalainen-Lindsberg ML, Pellinen T, Leppä S. Clinical Impact of Immune Cells and Their Spatial Interactions in Diffuse Large B-Cell Lymphoma Microenvironment. Clin Cancer Res. 2022;28(4):781-792.
13. Colombo AR, Hav M, Singh M, et al. Single-cell spatial analysis of tumor immune architecture in diffuse large B-cell lymphoma. Blood Adv. 2022;6(16):4675-4690.
14. Wright KT, Weirather JL, Jiang S, et al. Diffuse large B-cell lymphomas have spatially defined, tumor immune microenvironments revealed by high-parameter imaging. Blood Adv. 2023;7(16):4633-4646.
15. Ansell SM, Minnema MC, Johnson P, et al. Nivolumab for Relapsed/Refractory Diffuse Large B-Cell Lymphoma in Patients Ineligible for or Having Failed Autologous Transplantation: A Single-Arm, Phase II Study. J Clin Oncol. 2019;37(6):481-489.
16. Alizadeh AA, Eisen MB, Davis RE, et al. Distinct types of diffuse large B-cell lymphoma identified by gene expression profiling. Nature. 2000;403(6769):503-511.
17. Fu K, Weisenburger DD, Choi WW, et al. Addition of rituximab to standard chemotherapy improves the survival of both the germinal center B-cell-like and non-germinal center B-cell-like subtypes of diffuse large B-cell lymphoma. J Clin Oncol. 2008;26(28):4587-4594.
18. Lenz G, Wright G, Dave SS, et al. Stromal gene signatures in large-B-cell lymphomas. N Engl J Med. 2008;359(22):2313-2323.
19. Bea S, Zettl A, Wright G, et al. Diffuse large B-cell lymphoma subgroups have distinct genetic profiles that influence tumor biology and improve gene-expression-based survival prediction. Blood. 2005;106(9):3183-3190.
20. Pasqualucci L, Dalla-Favera R. Genetics of diffuse large B-cell lymphoma. Blood. 2018;131(21):2307-2319.

21. Davis RE, Brown KD, Siebenlist U, Staudt LM. Constitutive nuclear factor kappaB activity is required for survival of activated B cell-like diffuse large B cell lymphoma cells. J Exp Med. 2001;194(12):1861-1874.
22. Morin RD, Johnson NA, Severson TM, et al. Somatic mutations altering EZH2 (Tyr641) in follicular and diffuse large B-cell lymphomas of germinal-center origin. Nat Genet. 2010;42(2):181-185.
23. Rosenwald A, Wright G, Chan WC, et al. The use of molecular profiling to predict survival after chemotherapy for diffuse large-B-cell lymphoma. N Engl J Med. 2002;346(25):1937-1947.
24. Schmitz R, Wright GW, Huang DW, et al. Genetics and Pathogenesis of Diffuse Large B-Cell Lymphoma. N Engl J Med. 2018;378(15):1396-1407.
25. Chapuy B, Stewart C, Dunford AJ, et al. Molecular subtypes of diffuse large B cell lymphoma are associated with distinct pathogenic mechanisms and outcomes. Nat Med. 2018;24(5):679-690.
26. Cheah CY, Wirth A, Seymour JF. Primary testicular lymphoma. Blood. 2014;123(4):486-493.
27. Deng L, Xu-Monette ZY, Loghavi S, et al. Primary testicular diffuse large B-cell lymphoma displays distinct clinical and biological features for treatment failure in rituximab era: a report from the International PTL Consortium. Leukemia. 2016;30(2):361-372.
28. Leivonen SK, Pollari M, Bruck O, et al. T-cell inflamed tumor microenvironment predicts favorable prognosis in primary testicular lymphoma. Haematologica. 2019;104(2):338-346.
29. Holte H, Leppa S, Bjorkholm M, et al. Dose-densified chemoimmunotherapy followed by systemic central nervous system prophylaxis for younger high-risk diffuse large B-cell/follicular grade 3 lymphoma patients: results of a phase II Nordic Lymphoma Group study. Ann Oncol. 2013;24(5):1385-1392.
30. Leppä S, Jørgensen J, Tierens A, et al. Patients with high-risk DLBCL benefit from dose-dense immunochemotherapy combined with early systemic CNS prophylaxis. Blood Adv. 2020;4(9):1906-1915.
31. Meriranta L, Pasanen A, Alkodsi A, Haukka J, Karjalainen-Lindsberg ML, Leppä S. Molecular background delineates outcome of double protein expressor diffuse large B-cell lymphoma. Blood Adv. 2020;4(15):3742-3753.
32. Reddy A, Zhang J, Davis NS, et al. Genetic and Functional Drivers of Diffuse Large B Cell Lymphoma. Cell. 2017;171(2):481-494.e415.
33. Scott DW, Wright GW, Williams PM, et al. Determining cell-of-origin subtypes of diffuse large B-cell lymphoma using gene expression in formalin-fixed paraffin-embedded tissue. Blood. 2014;123(8):1214-1217.
34. Isaksen KT, Beiske K, Smeland EB, et al. The DLBCL90 gene-expression assay identifies double-hit lymphomas with high sensitivity in patients from two phase II clinical trials with high-risk diffuse large B-cell lymphoma. EJHaem. 2021;2(1):104-108.
35. Pollari M, Pellinen T, Karjalainen-Lindsberg ML, Kellokumpu-Lehtinen PL, Leivonen SK, Leppä S. Adverse prognostic impact of regulatory T-cells in testicular diffuse large B-cell lymphoma. Eur J Haematol. 2020;105(6):712-721.
36. Berg S, Kutra D, Kroeger T, et al. ilastik: interactive machine learning for (bio)image analysis. Nat Methods. 2019;16(12):1226-1232.
37. Carpenter AE, Jones TR, Lamprecht MR, et al. CellProfiler: image analysis software for identifying and quantifying cell phenotypes. Genome Biol. 2006;7(10):R100.
38. Brück O, Lee MH, Turkki R, et al. Spatial immunoprofiling of the intratumoral and peritumoral tissue of renal cell carcinoma patients. Mod Pathol. 2021;34(12):2229-2241.
39. Liarski VM, Sibley A, van Panhuys N, et al. Quantifying in situ adaptive immune cell cognate interactions in humans. Nat Immunol. 2019;20(4):503-513.
40. Pollari M, Bruck O, Pellinen T, et al. PD-L1(+) tumor-associated macrophages and PD-1(+) tumor-infiltrating lymphocytes predict survival in primary testicular lymphoma. Haematologica. 2018;103(11):1908-1914.
41. Dufva O, Pölönen P, Brück O, et al. Immunogenomic Landscape of Hematological Malignancies. Cancer Cell. 2020;38(3):380-399.e313.

42. Fangazio M, Ladewig E, Gomez K, et al. Genetic mechanisms of HLA-I loss and immune escape in diffuse large B cell lymphoma. Proc Natl Acad Sci U S A. 2021;118(22):e2104504118.
43. McCord R, Bolen CR, Koeppen H, et al. PD-L1 and tumor-associated macrophages in de novo DLBCL. Blood Adv. 2019;3(4):531-540.
44. Li L, Sun R, Miao Y, et al. PD-1/PD-L1 expression and interaction by automated quantitative immunofluorescent analysis show adverse prognostic impact in patients with diffuse large B-cell lymphoma having T-cell infiltration: a study from the International DLBCL Consortium Program. Mod Pathol. 2019;32(6):741-754.

Figure Legends

Figure 1. Differentially expressed immune-related genes between germinal center B-cell like (GCB) and activated B-cell like (ABC) diffuse large B-cell lymphoma (DLBCL). A) A volcano plot depicting differently expressed immune-related genes between ABC and GCB DLBCL in the DLBCL, not otherwise specified (NOS) gene expression cohort. B) Unsupervised hierarchical clustering of patients in the DLBCL, NOS gene expression cohort based on the expression of the 32 most differently expressed genes (adj. p<0.01) between ABC and GCB DLBCL.

Figure 2. The composition of the tumor microenvironment (TME) in germinal B-cell like (GCB) and activated B-cell like (ABC) diffuse large B-cell lymphoma (DLBCL) analyzed by multiplex immunohistochemistry (mIHC). A) Representative images of a GCB and ABC DLBCL sample from mIHC analyses performed on tissue microarrays (TMAs). CD3=red, CD4=cyan, CD68=blue, CD163=magenta, PD-1=green, PD-L1=yellow, DAPI=grey. Scale bars 150 µm and 50 µm in the left and right images, respectively. B) A volcano plot depicting immune cell types whose proportions in the TME differ most between ABC and GCB DLBCL in the DLBCL, not otherwise specified (NOS) mIHC cohort. Cell proportions indicate proportions of total cells except where stated otherwise. C-H) Boxplots depicting the proportions of M2-like macrophages/total cells (C), M1-like macrophages/macrophages (D), T helper cells/T cells (E), Regulatory T cells/T cells (F), GrB^+ T cells/T cells (G), and $PD\text{-}L1^+$ M2-like macrophages/total cells (H) in the TME of GCB and ABC DLBCL analyzed in the DLBCL, NOS mIHC cohort. Statistical significance was analyzed using the Mann-Whitney U test. Due to staining errors, data on certain cell types was unavailable for some samples. TAMs= $CD68^+$ cells, M2-like=$CD163^+$ cells, M1-like=$CD163^-CD68^+$ cells, T cells=$CD3^+$ cells, Th=$CD4^+CD3^+$ cells, Tc=$CD8^+$ cells, Tregs=$FOXP3^+CD3^+$ cells.

Figure 3. Differently expressed immune-related genes and differences in the constitution of the tumor microenvironment (TME) analyzed by multiplex immunohistochemistry (mIHC) between testicular diffuse large B-cell lymphoma (T-DLBCL) and DLBCL, not otherwise specified (NOS). A) A dot plot depicting the first two components of a principal component

analysis performed with all available immune-related genes in patients from the T-DLBCL and the DLBCL, NOS gene expression cohorts analyzed by Nanostring nCounter Human PanCancer Immunoprofiling Panel. B-E) Boxplots depicting the proportions of GrB^+ cells/total cells (B), M2-like macrophages/total cells (C), M1-like macrophages/total cells (D), and Tregs/T cells (E) in the TME of germinal center (GC) and non-GC T-DLBCL as well as GCB and ABC DLBCL samples in the T-DLBCL and DLBCL, NOS multiplex immunohistochemistry (mIHC) cohorts. The numbers comparing different subtypes are adj. *p*-values for the Mann-Whitney U test comparing the respective groups. Due to staining errors, data on certain cell types was unavailable for some samples. F) A barplot depicting the proportion of T-DLBCL and GCB and ABC type DLBCL, NOS samples staining positive for HLA-ABC, B2M, and HLA-DR analyzed by immunohistochemistry (IHC) in the T-DLBCL and DLBCL, NOS mIHC cohorts. T cells=$CD3^+$ cells, Tregs=$FOXP3^+CD4^+CD3^+$ cells, Tregs/T cells=$FOXP3^+CD3^+/CD3^+$ cells, M1-like=$CD163^-CD68^+$ cells, M2-like=$CD163^+$ cells.

Figure 4. Interactions between different immune cell subtypes in the tumor microenvironment (TME) of germinal B-cell like (GCB) and activated B-cell like (ABC) diffuse large B-cell lymphoma (DLBCL) and testicular (T)-DLBCL. Boxplots depicting differences in the number of selected significant interactions between different immune cells in GCB and ABC DLBCL, not otherwise specified (NOS) and T-DLBCL samples in the DLBCL, NOS and T-DLBCL multiplex immunohistochemistry (mIHC) cohorts. Th=$CD4^+CD3^+$ cells, Tc=$CD4^-CD3^+$ cells, M2=$CD163^+$ cells, M1=$CD163^-CD68^+$ cells, B cell=$CD20^+$ cells, PD1=$PD\text{-}1^+$ cells, PDL1=$PD\text{-}L1^+$ cells. * = adj. $p < 0.05$, ** = adj. $p < 0.01$, *** adj. $p < 0.001$, **** = adj. $p < 0.0001$.

Figure 5. Clinical impact of different immune cells and their interactions in the tumor microenvironment (TME) of germinal center B-cell like (GCB) and activated B-cell like (ABC) diffuse large B-cell lymphoma (DLBCL) and testicular (T)-DLBCL. A) A forest plot visualizing the impact of selected immune cell subtypes on progression-free survival (PFS) in GCB and ABC DLBCL in the DLBCL, NOS multiplex immunohistochemistry (mIHC) cohort, as evaluated by Cox univariable regression analyses with continuous variables. B) A forest plot visualizing the impact of

macrophages on PFS in a Cox multivariable regression analysis with International Prognostic Index (IPI) in patients with GCB DLBCL in the DLBCL, NOS mIHC cohort. C-D) Kaplan-Meier (log-rank test) survival plots depict PFS in GCB (C) and ABC DLBCL (D) patients with high and low proportions of macrophages using median cutoff in the DLBCL, NOS mIHC cohort. TAM=$CD68^+$ cells, M1= $CD163^-CD68^+$ cells, M2=$CD163^+$ cells, T cell=$CD3^+$ cells, Tc=$CD8^+$ cells.

Figure 6. Clinical impact of different immune cell interactions in the tumor microenvironment (TME) of germinal center B-cell like (GCB) and activated B-cell like (ABC) diffuse large B-cell lymphoma (DLBCL) and testicular (T)-DLBCL. A) A forest plot visualizing the impact of selected immune cell interactions on progression-free survival (PFS) in GCB and ABC DLBCL in the DLBCL, not otherwise specified (NOS) multiplex immunohistochemistry (mIHC) cohort, and in T-DLBCL in the T-DLBCL mIHC cohort, respectively, as evaluated by Cox univariable regression analyses with continuous variables. B) A forest plot visualizing the impact of M2-like macrophage-T cell interactions on PFS in a Cox multivariable regression analysis with IPI in patients with GCB DLBCL in the DLBCL, NOS mIHC cohort. C) A forest plot visualizing the impact of T helper cell-macrophage interactions on PFS in a Cox multivariable regression analysis with International Prognostic Index (IPI), molecular subtype, and treatment (rituximab-containing immunochemotherapy vs. chemotherapy) in patients with T-DLBCL in the T-DLBCL mIHC cohort. D) Kaplan-Meier (log-rank test) survival plot depicts PFS in T-DLBCL patients with high and low amounts of T helper cell-macrophage interactions in their TME using median cutoff in the T-DLBCL mIHC cohort. TAM=$CD68^+$ cells, M2=$CD163^+$ cells, T cell=$CD3^+$ cells, Th=$CD4^+CD3^+$ cells, PD1=PD-1^+ cells, ICT=Immunochemotherapy.

Figure 7. Summary of the differences in the composition of the tumor microenvironment (TME) in germinal center B-cell like (GCB) and activated B-cell like (ABC) type diffuse large B-cell lymphoma (DLBCL), not otherwise specified (NOS) and testicular (T)-DLBCL. Schematic diagram depicting the proportions of M2-like macrophages, M1-like macrophages, cytotoxicity, and T helper cells in GCB and ABC type DLBCL, NOS and T-DLBCL. Images were created using BioRender.com.

Figure 1

A

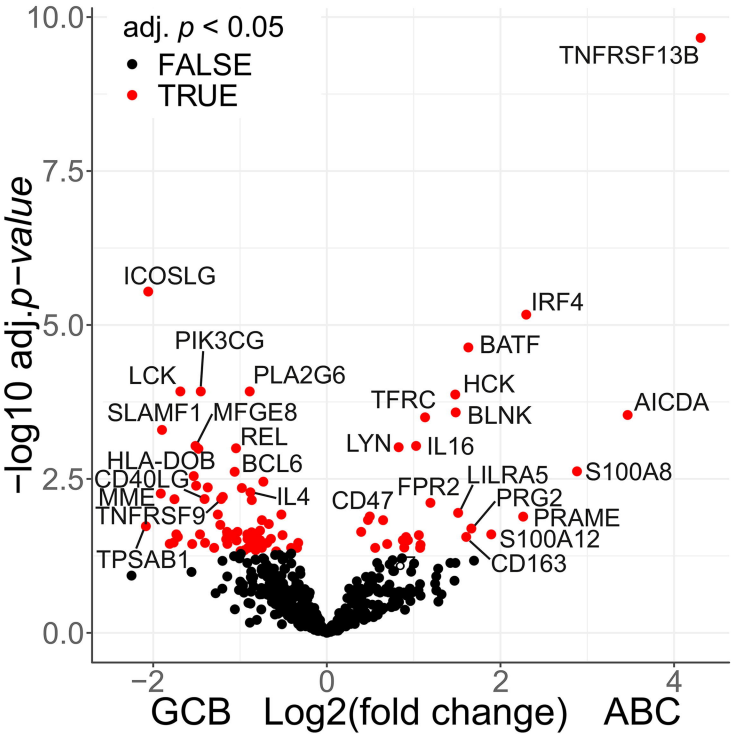
adj. p < 0.05
FALSE
TRUE
10.0
7.5
5.0
2.5
0.0
−log10 adj.p−value
−2
0
2
4
GCB Log2(fold change) ABC
TNFRSF13B
ICOSLG
IRF4
BATF
PIK3CG
LCK
PLA2G6
HCK
TFRC
BLNK
AICDA
SLAMF1
MFGE8
REL
LYN
IL16
HLA-DOB
BCL6
CD40LG
LILRA5
S100A8
MME
IL4
CD47
FPR2
PRG2
TNFRSF9
PRAME
S100A12
TPSAB1
CD163

B

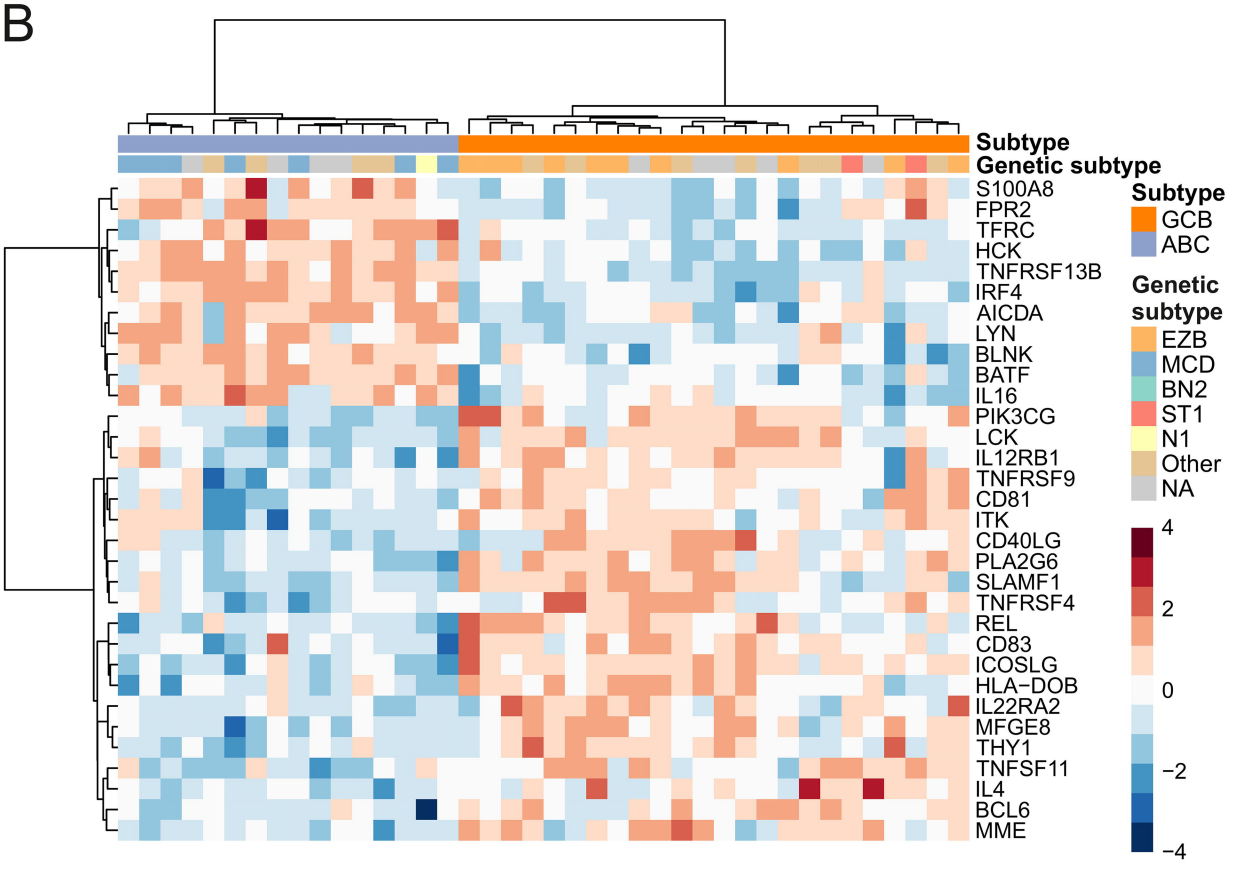
Subtype
Genetic subtype
S100A8
FPR2
TFRC
HCK
TNFRSF13B
IRF4
AICDA
LYN
BLNK
BATF
IL16
PIK3CG
LCK
IL12RB1
TNFRSF9
CD81
ITK
CD40LG
PLA2G6
SLAMF1
TNFRSF4
REL
CD83
ICOSLG
HLA−DOB
IL22RA2
MFGE8
THY1
TNFSF11
IL4
BCL6
MME
Subtype
GCB
ABC
Genetic subtype
EZB
MCD
BN2
ST1
N1
Other
NA
4
2
0
−2
−4

Figure 2

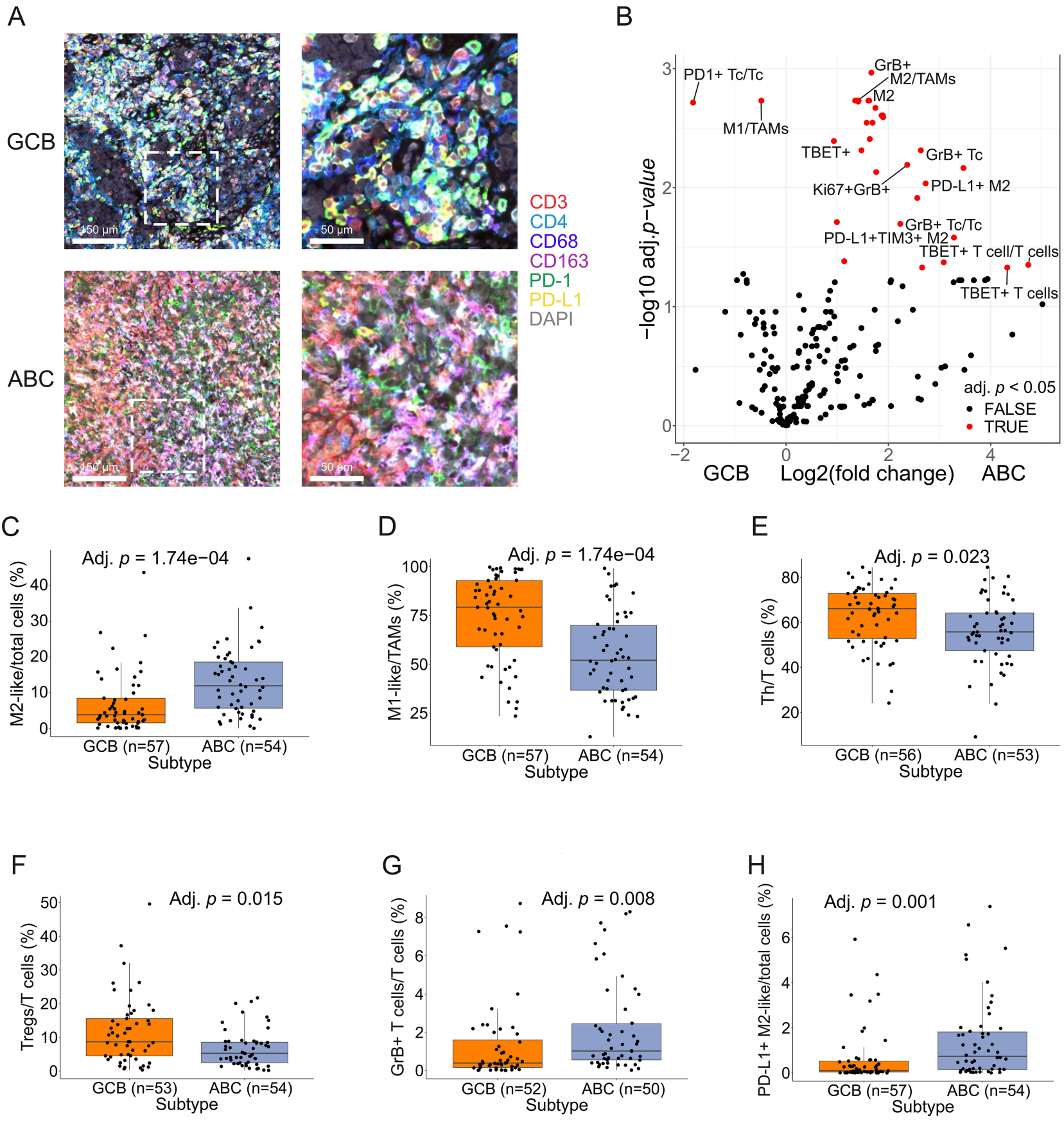
A
GCB
ABC
150 μm
50 μm
CD3
CD4
CD68
CD163
PD-1
PD-L1
DAPI
B
−log10 adj.p−value
Log2(fold change)
GCB
ABC
PD1+ Tc/Tc
GrB+
M2/TAMs
M2
M1/TAMs
TBET+
GrB+ Tc
Ki67+GrB+
PD-L1+ M2
GrB+ Tc/Tc
PD-L1+TIM3+ M2
TBET+ T cell/T cells
TBET+ T cells
adj. p < 0.05
FALSE
TRUE
C
Adj. p = 1.74e−04
M2-like/total cells (%)
GCB (n=57)
ABC (n=54)
Subtype
D
Adj. p = 1.74e−04
M1-like/TAMs (%)
GCB (n=57)
ABC (n=54)
Subtype
E
Adj. p = 0.023
Th/T cells (%)
GCB (n=56)
ABC (n=53)
Subtype
F
Adj. p = 0.015
Tregs/T cells (%)
GCB (n=53)
ABC (n=54)
Subtype
G
Adj. p = 0.008
GrB+ T cells/T cells (%)
GCB (n=52)
ABC (n=50)
Subtype
H
Adj. p = 0.001
PD-L1+ M2-like/total cells (%)
GCB (n=57)
ABC (n=54)
Subtype

Figure 3

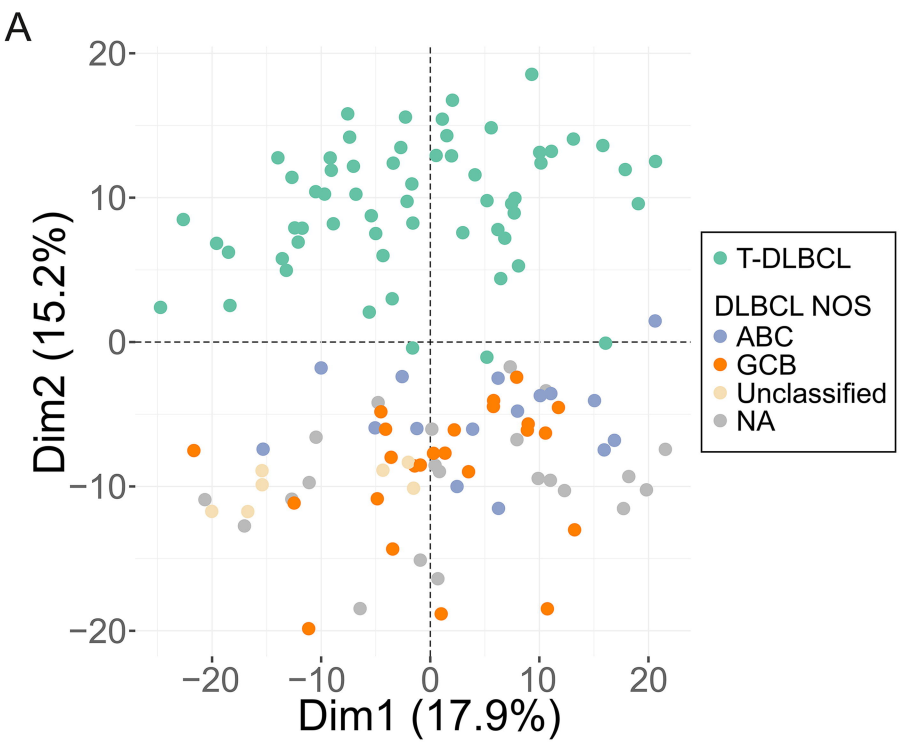
A
Dim2 (15.2%)
Dim1 (17.9%)
T-DLBCL
DLBCL NOS
ABC
GCB
Unclassified
NA

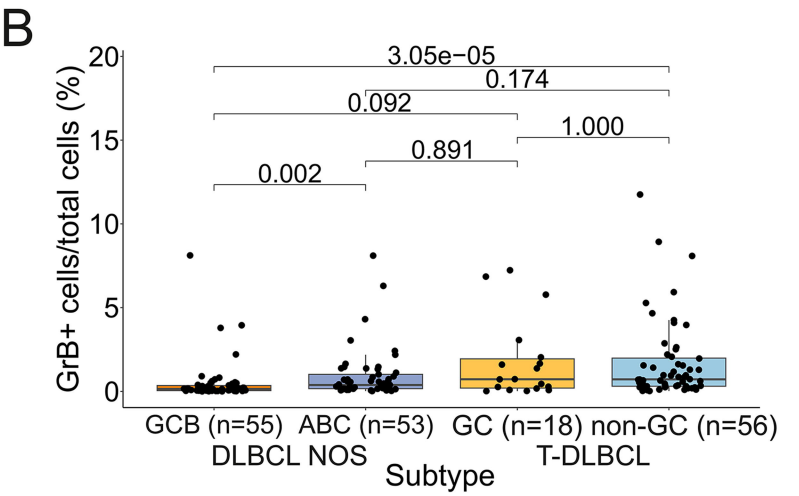
B
GrB+ cells/total cells (%)
3.05e−05
0.174
0.092
1.000
0.891
0.002
GCB (n=55)
ABC (n=53)
GC (n=18)
non-GC (n=56)
DLBCL NOS
T-DLBCL
Subtype

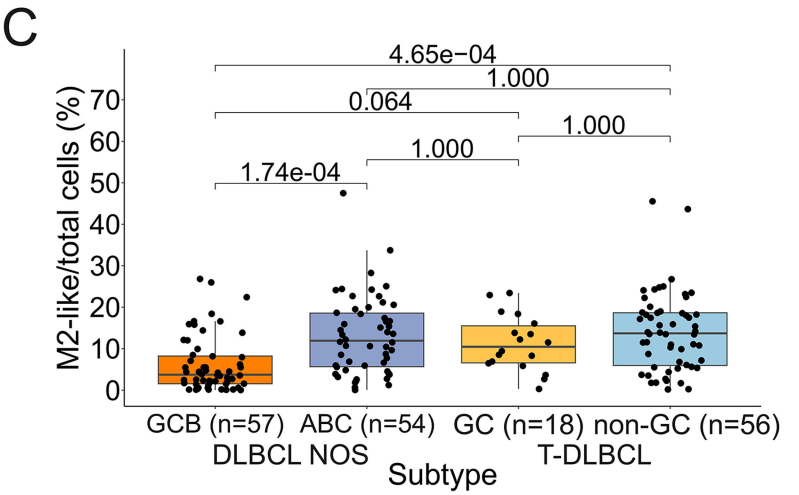
C
M2-like/total cells (%)
4.65e−04
1.000
0.064
1.000
1.000
1.74e-04
GCB (n=57)
ABC (n=54)
GC (n=18)
non-GC (n=56)
DLBCL NOS
T-DLBCL
Subtype

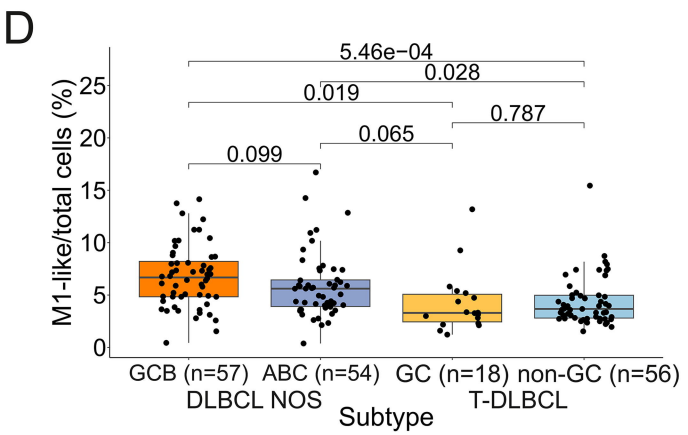
D
M1-like/total cells (%)
5.46e−04
0.028
0.019
0.787
0.065
0.099
GCB (n=57)
ABC (n=54)
GC (n=18)
non-GC (n=56)
DLBCL NOS
T-DLBCL
Subtype

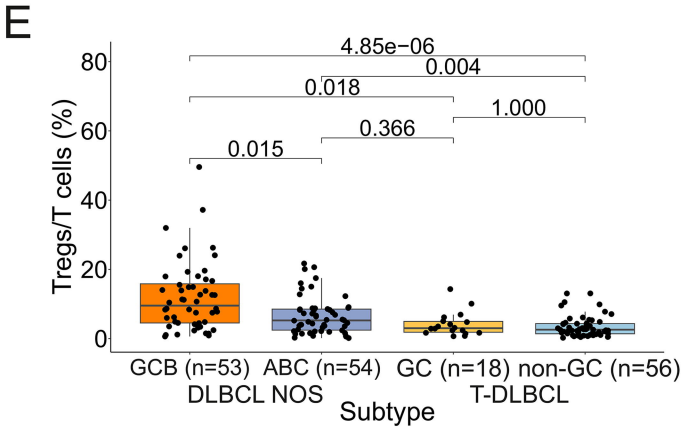
E
Tregs/T cells (%)
4.85e−06
0.004
0.018
1.000
0.366
0.015
GCB (n=53)
ABC (n=54)
GC (n=18)
non-GC (n=56)
DLBCL NOS
T-DLBCL
Subtype

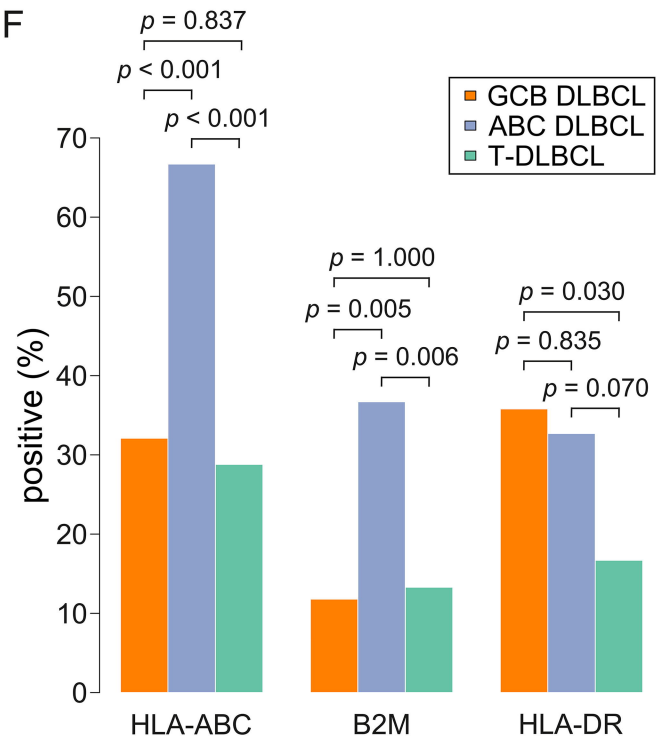
F
positive (%)
p = 0.837
p < 0.001
p < 0.001
p = 1.000
p = 0.005
p = 0.006
p = 0.030
p = 0.835
p = 0.070
GCB DLBCL
ABC DLBCL
T-DLBCL
HLA-ABC
B2M
HLA-DR

Figure 4

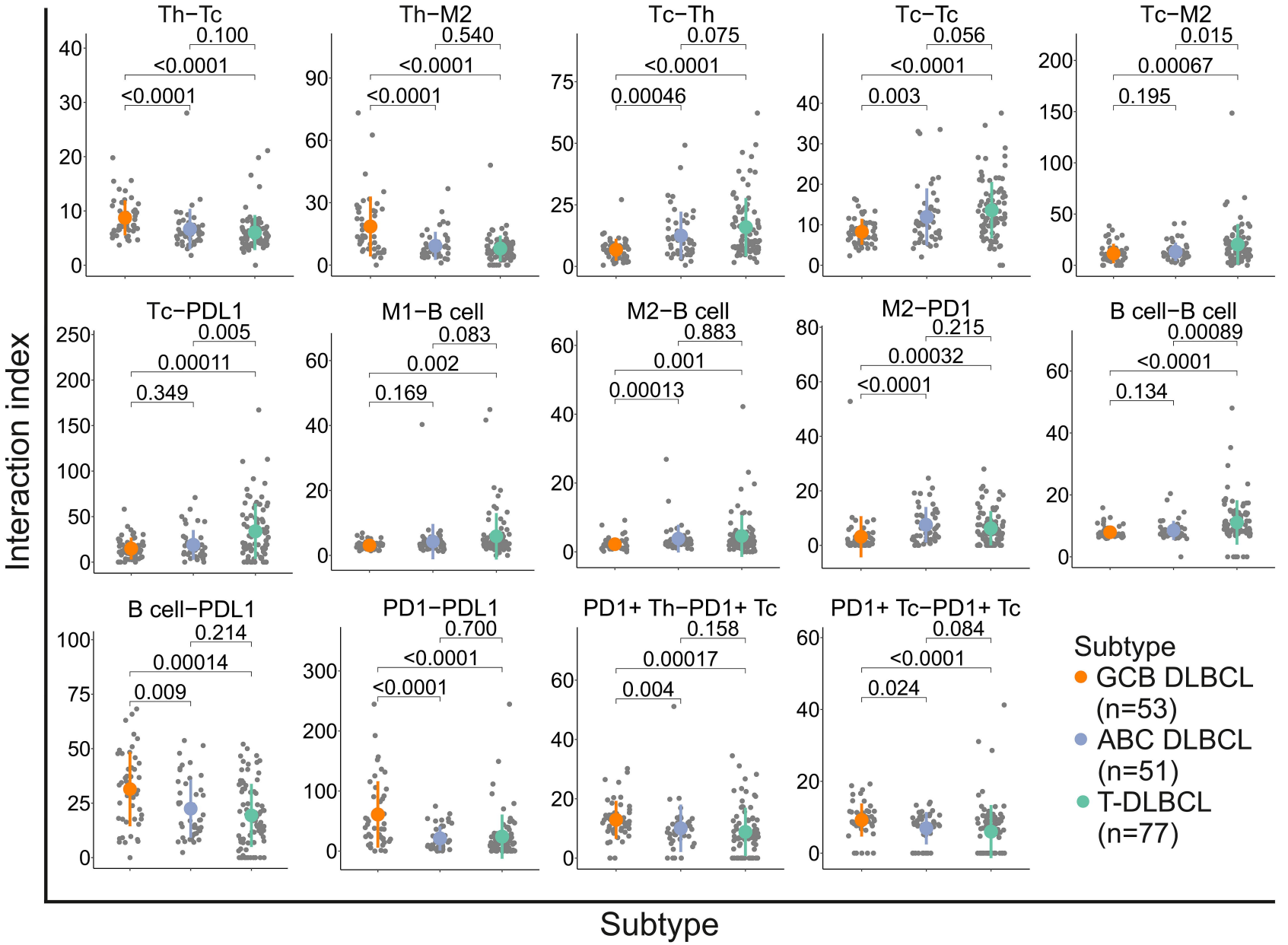
Th−Tc
0.100
<0.0001
<0.0001
Th−M2
0.540
<0.0001
<0.0001
Tc−Th
0.075
<0.0001
0.00046
Tc−Tc
0.056
<0.0001
0.003
Tc−M2
0.015
0.00067
0.195
Tc−PDL1
0.005
0.00011
0.349
M1−B cell
0.083
0.002
0.169
M2−B cell
0.883
0.001
0.00013
M2−PD1
0.215
0.00032
<0.0001
B cell−B cell
0.00089
<0.0001
0.134
B cell−PDL1
0.214
0.00014
0.009
PD1−PDL1
0.700
<0.0001
<0.0001
PD1+ Th−PD1+ Tc
0.158
0.00017
0.004
PD1+ Tc−PD1+ Tc
0.084
<0.0001
0.024
Interaction index
Subtype
Subtype
GCB DLBCL (n=53)
ABC DLBCL (n=51)
T-DLBCL (n=77)

Figure 5

A

GCB	PFS HR (95% CI)	p
PD−L1+TIM3+ M1 (n=49)	2.85 (1.07−7.62)	0.037
TAMs (n=57)	1.24 (1.03−1.49)	0.024
M2 (n=57)	1.06 (1.00−1.12)	0.050
PD−L1+ (n=57)	1.16 (1.01−1.34)	0.039
Granzyme B+ (n=55)	1.51 (1.06−2.14)	0.021
TIM3+ T cells (n=51)	1.23 (1.05−1.43)	0.010
Tc (n=55)	1.01 (0.89−1.15)	0.888
ABC		
PD−L1+TIM3+ M1 (n=52)	2.92 (1.05−8.14)	0.041
TAMs (n=54)	1.07 (0.96−1.18)	0.207
M2 (n=54)	0.99 (0.95−1.05)	0.831
PD−L1+ (n=54)	1.00 (0.92−1.08)	0.921
Granzyme B+ (n=53)	1.25 (0.98−1.60)	0.071
TIM3+ T cells (n=49)	1.02 (0.91−1.16)	0.700
Tc (n=57)	0.92 (0.84−1.00)	0.048

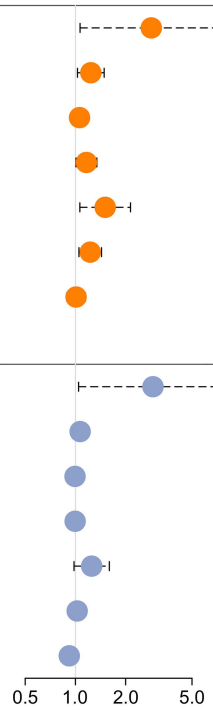

B

GCB	PFS HR (95% CI)	p
TAMs	1.24 (1.03−1.49)	0.026
IPI 3−5	0.98 (0.21−4.50)	0.976

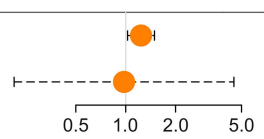

C

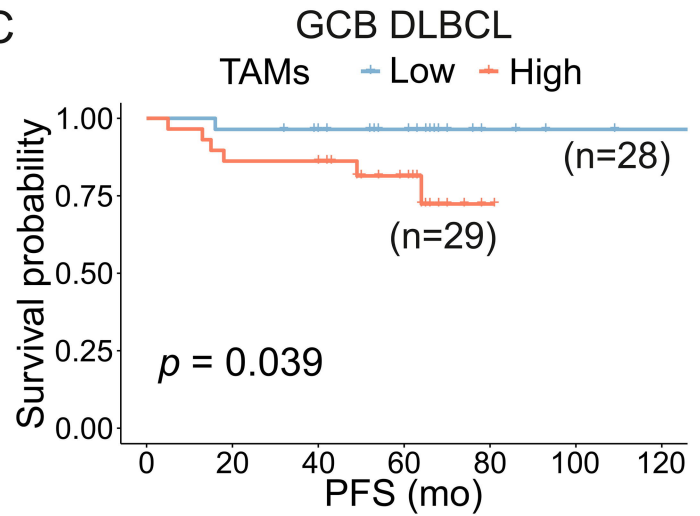

D

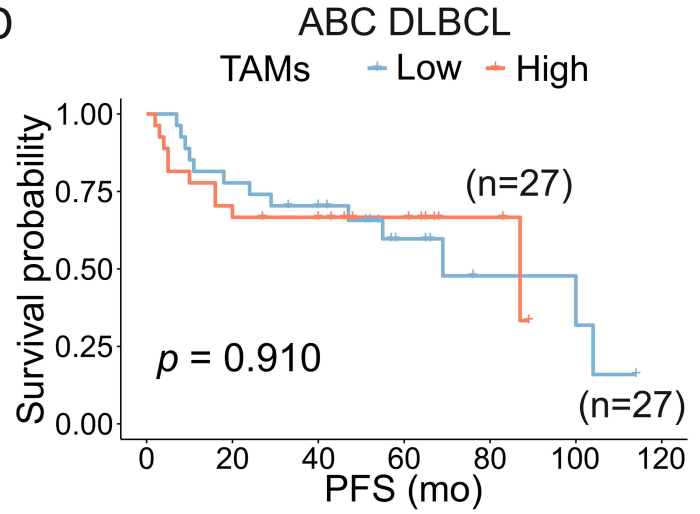

Figure 6

A

GCB (n=53)	PFS HR (95% CI)	p
M2−T cell	1.21 (1.05−1.39)	0.009
M2−Th	1.18 (1.04−1.34)	0.013
M2−PD1	1.05 (1.01−1.10)	0.016
T cell−TAM	0.94 (0.87−1.02)	0.122
Th−TAM	0.76 (0.55−1.06)	0.109
Th−T cell	1.28 (0.79−2.06)	0.318
ABC (n=51)		
M2−T cell	0.99 (0.88−1.10)	0.803
M2−Th	0.99 (0.93−1.05)	0.776
M2−PD1	0.96 (0.89−1.04)	0.308
T cell−TAM	0.96 (0.90−1.04)	0.316
Th−TAM	0.99 (0.87−1.14)	0.931
Th−T cell	1.07 (0.81−1.43)	0.625
T−DLBCL (n=76)		
M2−T cell	1.13 (1.03−1.24)	0.012
M2−Th	1.09 (1.01−1.18)	0.021
M2−PD1	1.05 (1.00−1.10)	0.043
T cell−TAM	0.91 (0.84−0.97)	0.005
Th−TAM	0.78 (0.67−0.90)	<0.001
Th−T cell	0.70 (0.54−0.91)	0.008

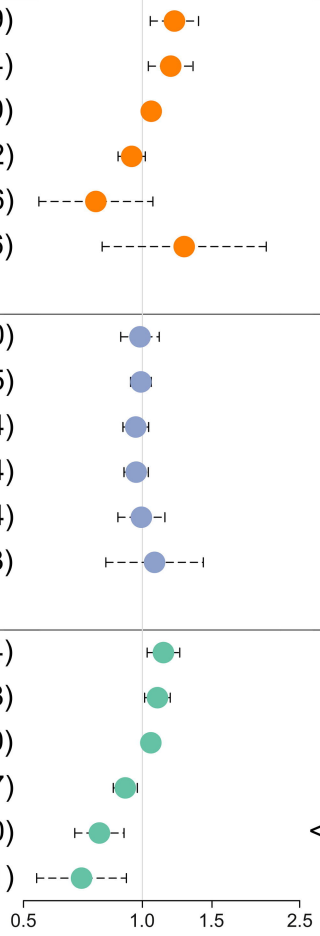

B

GCB	PFS HR (95% CI)	p
M2−T cell	1.22 (1.04−1.44)	0.013
IPI 3−5	0.63 (0.09−4.23)	0.637

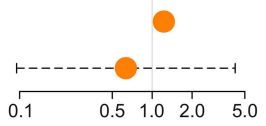

C

T-DLBCL	PFS HR (95% CI)	p
Th−TAM	0.82 (0.68−0.99)	0.036
IPI 3−5	7.58 (3.28−17.5)	<0.001
non−GC	4.24 (1.73−10.4)	0.002
ICT	0.32 (0.14−0.73)	0.007

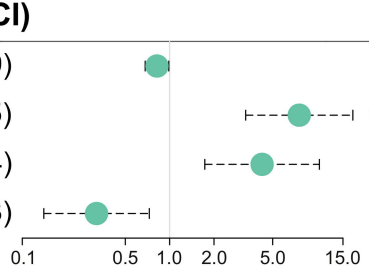

D

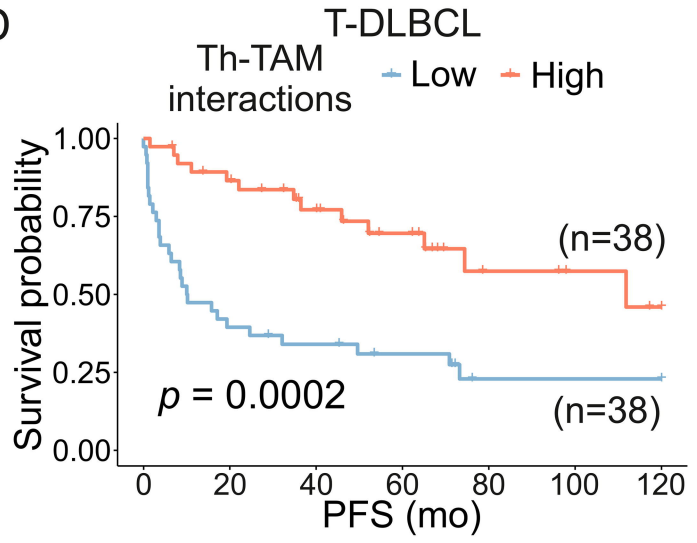

Figure 7

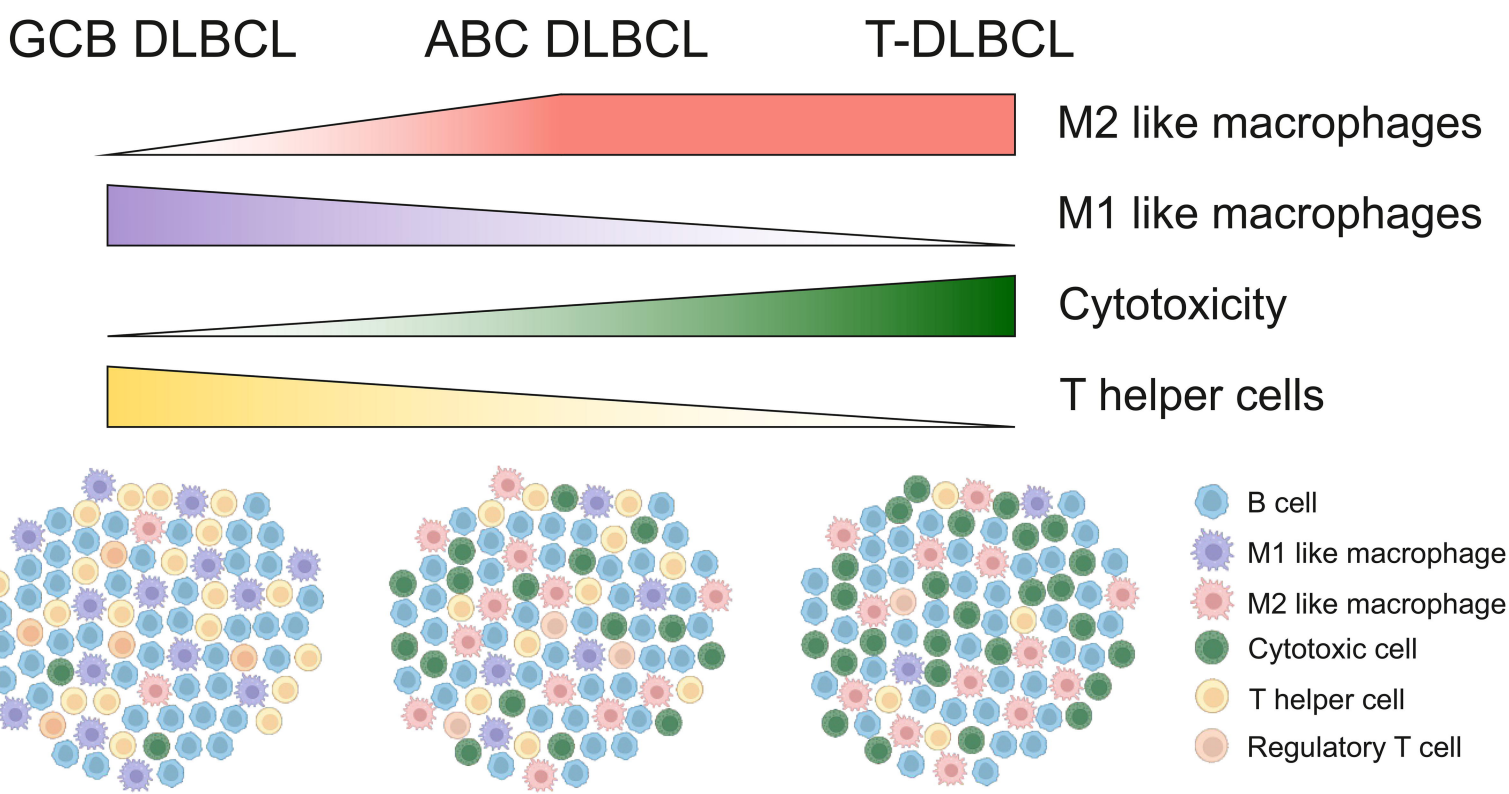
GCB DLBCL
ABC DLBCL
T-DLBCL
M2 like macrophages
M1 like macrophages
Cytotoxicity
T helper cells
B cell
M1 like macrophage
M2 like macrophage
Cytotoxic cell
T helper cell
Regulatory T cell

Characterization of tumor microenvironment and cell interaction patterns in testicular and diffuse large B-cell lymphomas

Autio et al.

Supplementary Materials and Methods

Methods

Multiplex IHC

Antibody staining panels

	Panel 1	**Panel 2**	**Panel 3**	**Panel 4**
TSA-488	R-anti-Granzyme B (Abcam;ab4059) 1:500	R-anti-Lag3 (Abcam;180187, clone EPR4392(2)) 1:400	M-anti-CD4 (Thermo;MA5-12259, clone 4B12) 1:50	M-anti-Tbet (Abcam;91109, clone 4B10) 1:50
TSA-555	M-anti-OX-40 (Thermo;14-1347-82, clone ACT35) 1:50	M-anti-PD-1 (LSBio;B12784, clone 3C6) 1:100	R-anti-CD3 (Thermo; MA5-14482, clone EP449E) 1:1500	R-anti-CD3 (Thermo; MA5-14482, clone EP449E) 1:1500
Alexa-647	R-anti-Ki67 (Thermo;9106-S0, clone SP6) 1:200	R-anti-Tim3 (CST[1];45208, clone D5D5R) 1:100	R-anti-Tim3 (CST;45208, clone D5D5R) 1:100	M-anti-FoxP3 (Abcam;20034, clone 236A/E7) 1:25
Alexa-750	M-anti-CD8 (Dako; M7103, clone C8/144B) 1:200	M-anti-CD8 (Dako; M7103, clone C8/144B) 1:200	M-anti-Lag3 (LSbio;C18692, clone 17B4) 1:50	R-anti-CD4 (Abcam;ab133616, clone EPR6855) 1:25
TSA-750			R-anti-CD4 (Abcam; Ab133616, clone EPR6855) 1:1000	

[1]CST, Cell Signaling Technologies

	Panel 5	**Panel 6**	**Panel 7**
1st round			
TSA-488	M-anti-CD68 (Abcam; ab955, clone KP1) 1:200	M-anti-PD-1 (LSBio; B12784, clone 3C6) 1:200	M-anti-CD3 (Abcam; ab17143, clone F7.2.38 1:100; 1,5h RT
TSA-555	R-anti-PD-L1 (CST[1]; 13684) 1:200	R-anti-PD-L1 (CST; 13684) 1:200	R-anti-CD56 (Cell Marque; 156R-95) 1:1000
Alexa-647	R-anti-Tim-3 (CST; 45208, clone D5D5R) 1:100	R-anti-CD4 (Abcam; ab133616, clone EPR6855) 1:50	R-anti-Tim-3 (CST; 45208, clone D5D5R 1:100
Alexa-750	M-anti-CD20 (Thermo; MS-340-s, clone L26) 1:50	M-anti-CD68 (Abcam; ab955, clone KP1) 1:50	M-anti-CD45 (Dako; M0701, clone 2B11 + PD7/26) 1:50
Bleach boil			
2nd round			
Alexa 647		M-anti-CD3 (Abcam; ab17143, clone F7.2.38) 1:50	
Alexa-750	R-anti-CD163 (Abcam; ab188571, clone EPR14643) 1:200	R-anti-CD163 (Abcam; ab188571, clone EPR14643) 1:200	R-anti-Granzyme B (Abcam; ab4059) 1:100

[1]CST, Cell Signaling Technologies

We performed multiplex immunohistochemistry (mIHC) as described earlier[1-3]. We used AlexaFluor488 and AlexaFluor555 channels amplified using tyramide signal amplification (TSA) (PerkinElmer, Waltham, MA) to detect two targets. We used AlexaFluor 647 and AlexaFluor750 fluorochrome-conjugated secondary antibodies without amplification to detect two other targets using a pair of primary antibodies raised in different species. We used DAPI to counterstain nuclei and mounted and applied coverslips on the slides. In panel 3, due to weak CD4 signal, we re-stained and TSA-amplified CD4 using TSA Biotin System (#NEL700A001KT, PerkinElmer) and Streptavidin, AlexaFluor™ 750 conjugate (S21384, Thermo Fischer Scientific). In panels 5-7, after

first-round staining and whole-slide imaging of the TMAs, we soaked the slides in wash buffer at 4°C to remove the coverslips. We then bleached the previous AlexaFluor staining by soaking the slides in TBS buffer containg 25mM NaOH and 4.5%. Finally, to denature the antibodies from the first-round staining, we heated the slides in 1mM Tris/ 10mM EDTA pH9 solution for 20 minutes at 99°C. We then performed a second-round staining using AlexaFluor647 and AlexaFluor750 secondary antibodies to detect one or two additional targets.

Imaging

We used Zeiss Axio Scan.Z1 with Zeiss 20X (0.8NA, M27) Plan-Apochromat objective, Hamamatsu ORCA-Flash 4.0 V2 Digital CMOS camera (16-bit; 0.325 µm/pixel resolution), and Zeiss Colibri.7 LED Light Source to acquire digital, fluorescence images of mIHC slides. Following filter specifications were used: DAPI cube (Zeiss Filter Set 02), FITC cube (Zeiss filter Set 38 HE), Cy3 cube (Chroma technology Corp 49004 ET CY3/R), Cy5 cube (Chrome Technology Corp 49006 ET CY5), Cy7 cube (Chrome Technology Corp 49007 ET CY7). After image acquisition, we converted images to 8-bit JPEG2000 format (95% quality for panels 1-4 and 100% quality for panels 5-7).

Image analysis

We filtered out areas with staining artefacts due to autofluorescence using Ilastik (version 1.3.3). We then used CellProfiler (version 3.1.8) to perform image analysis. We used pixel co-localization to determine cell classes. We thresholded each channel intensity using Adaptive Otsu. We used “MaskImage” to determine double or triple channel positive pixels, “MeasureImageAreaOccupied” to determine thresholded channel pixel areas and counted areal proportions by dividing the area with pixel area occupied by all the channels combined (ImageMath Add command). We used “ExportToSpreadsheet” to export cell class areas as CSV files. For slides stained with panels 5-7, we also performed cell interaction analyses. First, we used CellProfiler (version 3.1.8) to perform cell segmentation on fluorescence images of the mIHC slides converted to 8-bit JPEG2000 format

(100% quality). We used Adaptive Otsu to threshold each channel intensity. We separated clumped objects based on intensity. We determined the quality of TMA cores by visual inspection and excluded low quality cores (e.g. ruptured or folded tissue) from further analyses.

Cell interaction analyses

As previously described, we performed cell-cell interaction analyses on the samples stained with panels 5-7 using the method developed by Brück et al.[4]. After segmentation, we calculated the Euclidean distance between the center points of each cell. We defined interacting cells as cells situated closer than 100 pixels (22μm) from each other. We then calculated an interaction index I_{ab} using the formula:

$$I_{ab} = \frac{\sum_0^{ab} i_{ab}}{\sqrt{\frac{\sum a}{\sum c} \times \frac{\sum b}{\sum c}}}$$

where i_{ab} is the interaction between any two cells *a* and *b*, $\sum a$ is the sum of cells *a*, $\sum b$ is the sum of cells *b*, and $\sum c$ is the sum of all cells in the sample.

References

1. Autio M, Leivonen SK, Brück O, et al. Immune cell constitution in the tumor microenvironment predicts the outcome in diffuse large B-cell lymphoma. Haematologica. 2021;106(3):718-729.
2. Autio M, Leivonen SK, Brück O, Karjalainen-Lindsberg ML, Pellinen T, Leppä S. Clinical Impact of Immune Cells and Their Spatial Interactions in Diffuse Large B-Cell Lymphoma Microenvironment. Clin Cancer Res. 2022;28(4):781-792.
3. Pollari M, Pellinen T, Karjalainen-Lindsberg ML, Kellokumpu-Lehtinen PL, Leivonen SK, Leppä S. Adverse prognostic impact of regulatory T-cells in testicular diffuse large B-cell lymphoma. Eur J Haematol. 2020;105(6):712-721.
4. Brück O, Lee MH, Turkki R, et al. Spatial immunoprofiling of the intratumoral and peritumoral tissue of renal cell carcinoma patients. Mod Pathol. 2021;34(12):2229-2241.
5. Reddy A, Zhang J, Davis NS, et al. Genetic and Functional Drivers of Diffuse Large B Cell Lymphoma. Cell. 2017;171(2):481-494.e415.
6. Kotlov N, Bagaev A, Revuelta MV, et al. Clinical and Biological Subtypes of B-cell Lymphoma Revealed by Microenvironmental Signatures. Cancer Discov. 2021;11(6):1468-1489.
7. Schmitz R, Wright GW, Huang DW, et al. Genetics and Pathogenesis of Diffuse Large B-Cell Lymphoma. N Engl J Med. 2018;378(15):1396-1407.

Supplementary Tables

Table S1. Patient characteristics

Characteristics	DLBCL, NOS GE cohort n (%)*	DLBCL, NOS mIHC cohort n (%)	T-DLBCL GE cohort n (%)	T-DLBCL mIHC cohort n (%)	Reddy et al. cohort n (%)
No of patients	69 (100)	175 (100)	60 (100)	80 (100)	496 (100)
Age					
median (range)	55 (22-65)	61 (16-84)	69 (36-83)	70 (36-92)	
<60	46 (67)	83 (47)	16 (27)	17 (21)	205 (41)
≥60	23 (33)	92 (53)	44 (73)	62 (78)	268 (54)
nd				1 (1)	23 (5)
Sex					
Male	49 (71)	102 (58)	60 (100)	80 (100)	270 (54)
Female	20 (29)	73 (42)			226 (46)
Cell-of-origin					
GCB†	24 (35)	61 (35)			217 (44)
ABC	16 (23)	58 (33)			203 (41)
Unclassified	7 (10)	18 (10)			76 (15)
nd	22 (32)	38 (22)	60 (100)	80 (100)	
Subtype (Hans algorithm)					
GC	30 (43)	73 (42)	15 (25)	18 (23)	
non-GC	24 (35)	84 (48)	40 (67)	56 (70)	
nd	15 (22)	18 (10)	5 (8)	6 (8)	496 (100)
Genetic subtype					
EZB	11 (16)	17 (10)			
MCD	7 (10)	14 (8)			
BN2	1 (1)	11 (6)			
ST2	4 (6)	11 (6)			
N1	1 (1)	1 (1)			
Other	17 (25)	58 (33)			
nd	28 (41)	63 (36)	60 (100)	80 (100)	496 (100)
WHO PS					
0-1	41 (59)	123 (70)	52 (87)	61 (76)	349 (70)
≥2	28 (41)	50 (29)	8 (13)	14 (18)	112 (23)
nd		2 (1)		5 (6)	35 (7)
Stage					
I-II	8 (12)	79 (45)	39 (65)	49 (61)	179 (36)
III-IV	61 (88)	95 (54)	21 (35)	27 (34)	307 (62)
nd		1 (1)		4 (5)	10 (2)
IPI					
0-2	18 (26)	94 (54)	42 (70)	52 (65)	212 (43)
3-5	51 (74)	78 (45)	18 (30)	23 (29)	176 (35)
nd		3 (2)		5 (6)	108 (22)
Elevated LDH					
Yes	60 (87)	108 (62)	22 (37)	25 (31)	235 (47)
No	9 (13)	65 (37)	38 (63)	48 (60)	206 (42)
nd		2 (1)		7 (9)	55 (11)
EN					
0-1	25 (36)	124 (71)	47 (78)	58 (73)	341 (69)
≥2	44 (64)	45 (26)	13 (22)	17 (21)	123 (25)
nd		6 (3)		5 (6)	32 (6)
B-symptoms					
Yes	46 (67)	58 (33)	12 (20)	13 (16)	
No	23 (33)	107 (61)	48 (80)	64 (80)	
nd		10 (6)		3 (4)	
Treatment					
R-CHOP		119 (68)	32 (53)	36 (45)	
R-CHOEP‡	69 (100)	53 (30)			
other		3 (2)	28 (47)	43 (54)	
nd				1 (1)	
5-year PFS	86 %	76 %	58 %	51 %	
5-year OS	88 %	79 %	60 %	54 %	63 %

*GE, gene expression

†GCB, germinal center B-cell like; ABC, activated B-cell like; nd, not determined; IPI, international prognostic index; LDH, lactate dehydrogenase; EN, extranodal site; R-CHOP, rituximab, cyclophosphamide, doxorubicin, vincristine, prednisone; R-CHOEP, R-CHOP + etoposide
‡Patients <65 y with high-risk features were treated with R-CHOEP-14 and systemic CNS prophylaxis consisting of high-dose methotrexate and high-dose cytarabine

Table S2. Analyzed cell subtypes and their immunophenotypes.

Cell type	Immunophenotype
B cells	CD20+
T cells (TIL)	CD3+
T helper cells (Th)	CD4+CD3+
Cytotoxic T cells (Tc)	CD8+
Regulatory T cells (Treg)	Foxp3+CD4+CD3+
Macrophages (TAM)	CD68+
M1-like macrophages (M1)	CD68+CD163-
M2-like macrophages (M2)	CD163+
NK cells	CD56+CD3-CD45+

Table S3. Differentially expressed immune-related genes in ABC DLBCLs compared to GCB DLBCLs in the DLBCL, NOS gene expression cohort. Please see separate excel file.

Table S4. Differentially expressed immune-related genes in ABC DLBCLs compared to GCB DLBCLs in the Reddy et al. cohort. Please see separate excel file.

Table S5. The proportions of immune cell types in ABC DLBCLs compared to GCB DLBCLs in the DLBCL, NOS mIHC cohort. Please see separate excel file.

Table S6. Differentially expressed immune-related genes in T-DLBCLs compared to DLBCL, NOSes in the T-DLBCL and DLBCL, NOS gene expression cohorts. Please see separate excel file.

Table S7. The proportion of immune cell types in T-DLBCLs compared to DLBCL, NOSes in the mIHC cohorts. Please see separate excel file.

Supplementary Figure Legends

Figure S1. Expression of immune-related genes in germinal center B-cell like (GCB) and activated B-cell like (ABC) diffuse large B-cell lymphoma (DLBCL). A) A volcano plot depicting differently expressed immune-related genes between ABC and GCB DLBCL in the Reddy et al. cohort[5]. B) Unsupervised hierarchical clustering of patients in the Reddy et al. cohort based on the expression of the 32 most differently expressed genes between ABC and GCB DLBCL identified in the DLBCL, not otherwise specified (NOS) gene expression cohort. C-P) Boxplots depicting the expressions of *CD163* (C), *GZMB* (D), *GZMH* (E), *GZMM* (F), *PRF1* (G), *CD3D* (H), *CD3E* (I), *CD3G* (J), *CD4* (K), *CD8A* (L), *CD8B* (M), *FOXP3* (N), *TBX21* (O), and *MS4A1* (P) in GCB and ABC DLBCL in the Reddy et al. cohort. Statistical significance was analyzed using Mann-Whitney U test. LME, Lymphoma microenvironment subtypes[6].

Figure S2. Differentially expressed immune-related genes between germinal center B-cell like (GCB) and activated B-cell like (ABC) diffuse large B-cell lymphoma (DLBCL) in the Schmitz et al. cohort[7]. A) A volcano plot depicting differently expressed immune-related genes between ABC and GCB DLBCL. B) Unsupervised hierarchical clustering of patients in the Schmitz et al. cohort based on the expression of the 32 most differently expressed genes between ABC and GCB DLBCL identified in the DLBCL, not otherwise specified (NOS) gene expression cohort.

Figure S3. Proportions of immune cell subtypes in germinal center B-cell like (GCB) and activated B-cell like (ABC) diffuse large B-cell lymphoma (DLBCL) analyzed by multiplex immunohistochemistry (mIHC). A-J) Boxplots depicting the proportions of T cells/total cells (A), T helper cells/total cells (B), cytotoxic T cells/total cells (C), GrB^+ cells/total cells (D), $PD\text{-}L1^+$ cells/total cells (E), $TIM3^+$ M2-like macrophages/total cells (F), $TIM3^+$ T cells/total cells (G), $PD\text{-}1^+$ T cells/total cells (H), $PD\text{-}1^+$ T helper cells/total cells (I), and $CD20^-$ cells/total cells (J) in GCB and

ABC DLBCL analyzed by mIHC in the DLBCL, not otherwise specified (NOS) mIHC cohort. Statistical significance was analyzed using Mann-Whitney U test. Due to staining errors, data on certain cell types was unavailable for some samples. K) A barplot depicting the proportion of GCB and ABC DLBCL samples staining positive for HLA-ABC, B2M, and HLA-DR analyzed by IHC in the DLBCL, NOS mIHC cohort. Statistical significance was analyzed using Mann-Whitney U test. Due to staining errors, data on certain cell types was unavailable for some samples. T cells=$CD3^+$ cells, Th cells=$CD4^+CD3^+$ cells, Tc cells=$CD8^+$ cells, M2-like=$CD163^+$ cells.

Figure S4. Proportions of immune cells in HLA and B2M positive and negative diffuse large B-cell lymphomas (DLBCLs). A-C) Boxplots depicting the proportions of immune cell subtypes in HLA-ABC (A), B2M (B), and HLA-DR (C) negative and positive DLBCL samples analyzed by multiplex immunohistochemistry (mIHC) in the DLBCL, not otherwise specified (NOS) mIHC cohort. Statistical significance was analyzed using Mann-Whitney U test. Due to staining errors, data on certain cell types was unavailable for some samples. T cells=$CD3^+$ cells, Th cells=$CD4^+CD3^+$ cells, Tc cells=$CD8^+$ cells, Tregs=$FOXP3^+CD3^+$ cells, TAMs=$CD68^+$ cells, M2-like=$CD163^+$ cells, M1-like=$CD163^-CD68^+$ cells, NK cells=$CD56^+CD3^-CD45^+$ cells.

Figure S5. Differently expressed immune-related genes between testicular diffuse large B-cell lymphoma (T-DLBCL) and DLBCL, not otherwise specified (NOS). A) Unsupervised hierarchical clustering of patients in the T-DLBCL and DLBCL, NOS gene expression cohorts based on the expression of all available immune-related genes. B) A volcano plot depicting differently expressed immune-related genes between T-DLBCL and DLBCL, NOS samples in the T-DLBCL and DLBCL, NOS gene expression cohorts analyzed by Nanostring nCounter Human PanCancer Immunoprofiling Panel. C) A volcano plot depicting immune cell types whose proportions in the TME differ most between T-DLBCL and DLBCL, NOS samples in the T-DLBCL and DLBCL, NOS mIHC cohorts. Cell proportions indicate proportions of total cells except where

stated otherwise. T cells=$CD3^+$ cells, Th=$CD4^+CD3^+$ cells, Tc=$CD8^+$ cells, Tregs=$FOXP3^+CD4^+CD3^+$ cells, Tregs/T cells=$FOXP3^+CD3^+/CD3^+$ cells, B cells=$CD20^+$ cells.

Figure S6. Differences in the constitution of the tumor microenvironment (TME) analyzed by multiplex immunohistochemistry (mIHC) between testicular diffuse large B-cell lymphoma (T-DLBCL) and DLBCL, not otherwise specified (NOS). A-L) Boxplots depicting the proportions of B cells/total cells (A), T cells/total cells (B), T helper cells/total cells (C), cytotoxic T cells/total cells (D), regulatory T cells/total cells (E), GrB^+ cells/total cells (F), macrophages/total cells (G), M1-like macrophages/total cells (H), M2-like macrophages/total cells (I), PD-1^+ cells/total cells (J), PD-1^+ T cells/total cells (K), and $LAG3^+$ T cells/total cells (L) in T-DLBCL and DLBCL, NOS samples in the T-DLBCL and DLBCL, NOS mIHC cohorts. Statistical significance was analyzed using Mann-Whitney U test. Due to staining errors, data on certain cell types was unavailable for some samples. M-U) Boxplots depicting the proportions of B cells/total cells (M), T cells/total cells (N), T helper cells/total cells (O), cytotoxic T cells/total cells (P), regulatory T cells/total cells (Q), GrB^+ cells/total cells (O), macrophages/total cells (R), PD-1^+ cells/total cells (S), PD-1^+ T cells/total cells (T), and $LAG3^+$ T cells/total cells (U) in germinal center (GC) and non-GC T-DLBCL as well as GCB and ABC DLBCL samples in the T-DLBCL and DLBCL, NOS mIHC cohorts. The numbers comparing different subtypes are adj. *p*-values for the Mann-Whitney U test comparing the respective groups. Due to staining errors, data on certain cell types was unavailable for some samples. V) A barplot depicting the proportion of T-DLBCL and GCB and ABC type DLBCL, NOS samples staining positive for HLA-ABC, B2M, and HLA-DR analyzed by IHC in the T-DLBCL and DLBCL, NOS mIHC cohorts. B cells=$CD20^+$ cells, T cells=$CD3^+$ cells, Th cells=$CD4^+CD3^+$ cells, Tc cells=$CD8^+$ cells, Tregs=$FOXP3^+CD3^+$ cells, TAMs=$CD68^+$ cells, M1-like=$CD163^-CD68^+$ cells.

Figure S7. Interactions between different immune cell subtypes in germinal center B-cell like (GCB) and activated B-cell like (ABC) diffuse large B-cell lymphoma (DLBCL) and

testicular (T)-DLBCL. A) Ballon plot depicting differences in the number of interactions between different immune cell subtypes in ABC compared to GCB DLBCL in the DLBCL, not otherwise specified (NOS) multiplex immunohistochemistry (mIHC) cohort. On the x-axis are depicted the studied cell phenotypes and, on the y-axis, their neighboring cell phenotypes. The color of the balloons shows the difference in the interaction index in ABC compared to GCB DLBCL, calculated as the 2-fold logarithm of the fold-change (FC). B) Boxplots depicting differences in the number of selected interactions between different immune cell subtypes in GCB and ABC DLBCL in the DLBCL, NOS mIHC cohort. C) Ballon plot depicting differences in the number of interactions between different immune cell subtypes in T-DLBCL compared to DLBCL, NOS samples in the DLBCL, NOS and T-DLBCL mIHC cohorts. On the x-axis are depicted the studied cell phenotypes and, on the y-axis, their neighboring cell phenotypes. The color of the balloons shows the difference in the interaction index in T-DLBCL samples compared to DLBCL, NOS samples, calculated as the 2-fold logarithm of the fold-change (FC). D) Boxplots depicting differences in the number of selected interactions between different immune cell subtypes in DLBCL, NOS and T-DLBCL samples in the DLBCL, NOS and T-DLBCL mIHC cohorts. TAM=$CD68^+$ cells, M1=$CD163^-$ $CD68^+$ cells, M2=$CD163^+$ cells, T cell=$CD3^+$ cells, B cell=$CD20^+$ cells, PD1=PD-1^+ cells, PDL1=PD-$L1^+$ cells, TIM3=$TIM3^+$ cells. * = adj. $p < 0.05$, ** = adj. $p < 0.01$, *** = adj. $p < 0.001$, ns = not significant.

Figure S8. Clinical impact of different immune cells and their interactions in germinal center B-cell like (GCB) and activated B-cell like (ABC) diffuse large B-cell lymphoma (DLBCL) and testicular (T)-DLBCL. A) A forest plot visualizing the impact of selected immune cell subtypes on overall survival (OS) in GCB and ABC DLBCL in the DLBCL, not otherwise specified (NOS) multiplex immunohistochemistry (mIHC) cohort, as evaluated by Cox univariable regression analyses with continuous variables. Due to staining errors, data on certain cell types was unavailable for some samples. B-G) Forest plots visualizing the impact of PD-$L1^+TIM3^+$ M1-like macrophages (B), macrophages (C), M2-like macrophages (D), PD-$L1^+$ cells (E), Granzyme B^+

cells (F), and TIM3+ T cells (G) on progression-free survival (PFS) and OS in Cox multivariable regression analyses with International Prognostic Index (IPI) in patients with GCB DLBCL in the DLBCL, NOS mIHC cohort. H-I) Kaplan-Meier (log-rank test) survival plots depict OS in GCB (H) and ABC DLBCL (I) patients with high and low proportions of macrophages using median cutoff in the DLBCL, NOS mIHC cohort. J-K) Forest plots visualizing the impact of PD-L1^{+}TIM3^{+} M1-like macrophages (J) and cytotoxic T cells (K) on PFS and OS in Cox multivariable regression analyses with IPI in patients with ABC DLBCL in the DLBCL, NOS mIHC cohort. TAMs=CD68^{+} cells, M1-like= CD163^{-}CD68^{+} cells, M2-like=CD163^{+} cells, T cells=CD3^{+} cells, Tc=CD8^{+} cells.

Figure S9. Clinical impact of different immune cell interactions in germinal center B-cell like (GCB) and activated B-cell like (ABC) diffuse large B-cell lymphoma (DLBCL) and testicular (T)-DLBCL. A) A forest visualizing the impact of selected immune cell interactions on overall survival (OS) in GCB and ABC DLBCL in the DLBCL, not otherwise specified (NOS) multiplex immunohistochemistry (mIHC) cohort, and in T-DLBCL in the T-DLBCL mIHC cohort, respectively, as evaluated by Cox univariable regression analyses with continuous variables. B-D) Forest plots visualizing the impact of M2-like macrophage-T cell interactions (B), M2-like macrophage-T helper cell interactions (C), and M2-like macrophage-PD1 interactions (D) on progression-free survival (PFS) and OS in Cox multivariable regression analyses with International Prognostic Index (IPI) in patients with GCB DLBCL in the DLBCL, NOS mIHC cohort. E-J) Forest plots visualizing the impact of M2-like macrophage-T cell interactions (E), M2-like macrophage-T helper cell interactions (F), M2-like macrophage-PD1 interactions (G), T cell-macrophage interactions (H), T helper cell-macrophage interactions (I), and T helper cell-T cell interactions (J) on PFS and OS in Cox multivariable regression analyses with IPI, molecular subtype, and treatment (rituximab containing immunochemotherapy vs. chemotherapy) in patients with T-DLBCL in the T-DLBCL mIHC cohort. K) Kaplan-Meier (log-rank test) survival plot depicts OS in T-DLBCL patients with high and low amounts of T-helper cell-macrophage interactions in their tumor microenvironment (TME) using median cutoff in the T-DLBCL mIHC cohort. L-M) Kaplan-Meier (log-rank test) survival

plots depict OS (L) and PFS (M) in T-DLBCL patients treated with R-CHOP-like immunochemotherapy with high and low amounts of T-helper cell-macrophage interactions in their TME using median cutoff in the T-DLBCL mIHC cohort. TAM=$CD68^+$ cells, M2=$CD163^+$ cells, T cell=$CD3^+$ cells, Th=$CD4^+CD3^+$ cells, PD1=PD-1^+ cells.

Figure S1. Expression of immune-related genes in germinal center B-cell like (GCB) and activated B-cell like (ABC) diffuse large B-cell lymphoma (DLBCL).

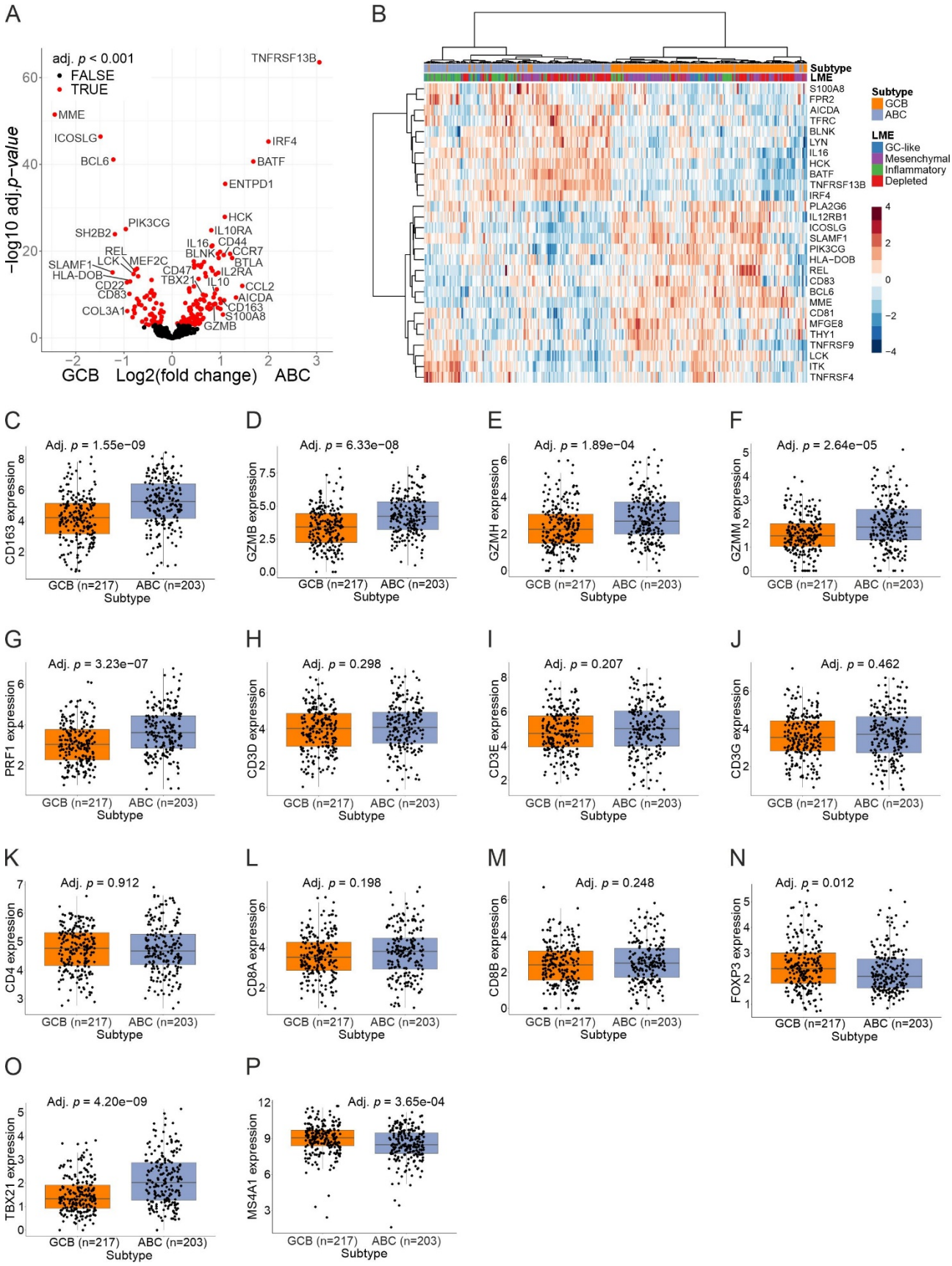

Figure S2. Differentially expressed immune-related genes between germinal center B-cell like (GCB) and activated B-cell like (ABC) diffuse large B-cell lymphoma (DLBCL) in the Schmitz et al. cohort[7].

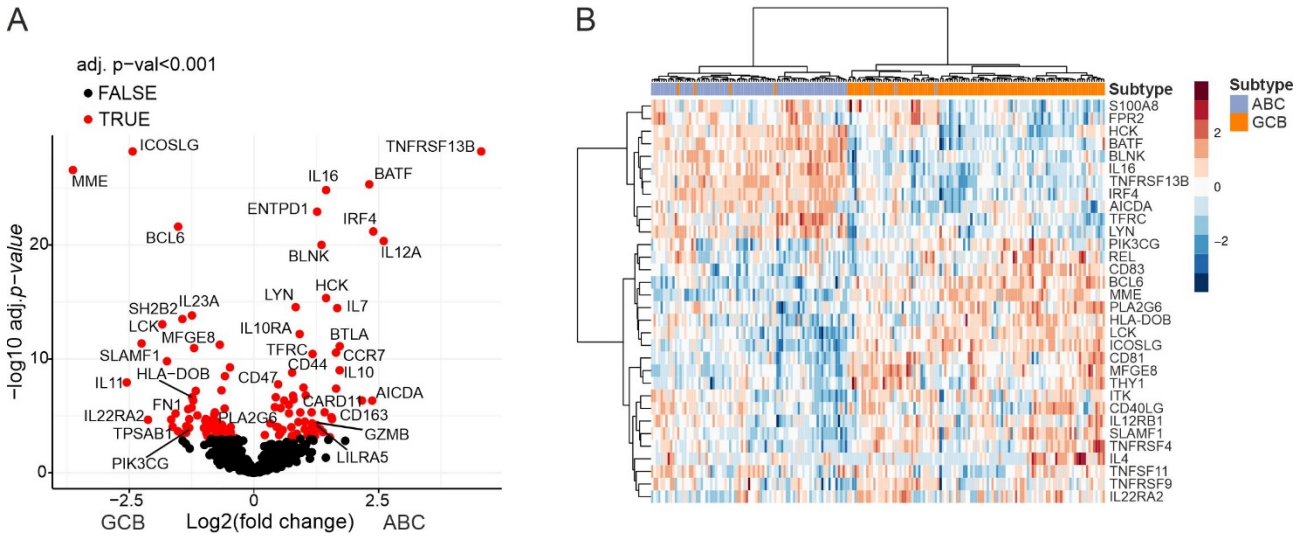

Figure S3. Proportions of immune cell subtypes in germinal center B-cell like (GCB) and activated B-cell like (ABC) diffuse large B-cell lymphoma (DLBCL) analyzed by multiplex immunohistochemistry (mIHC).

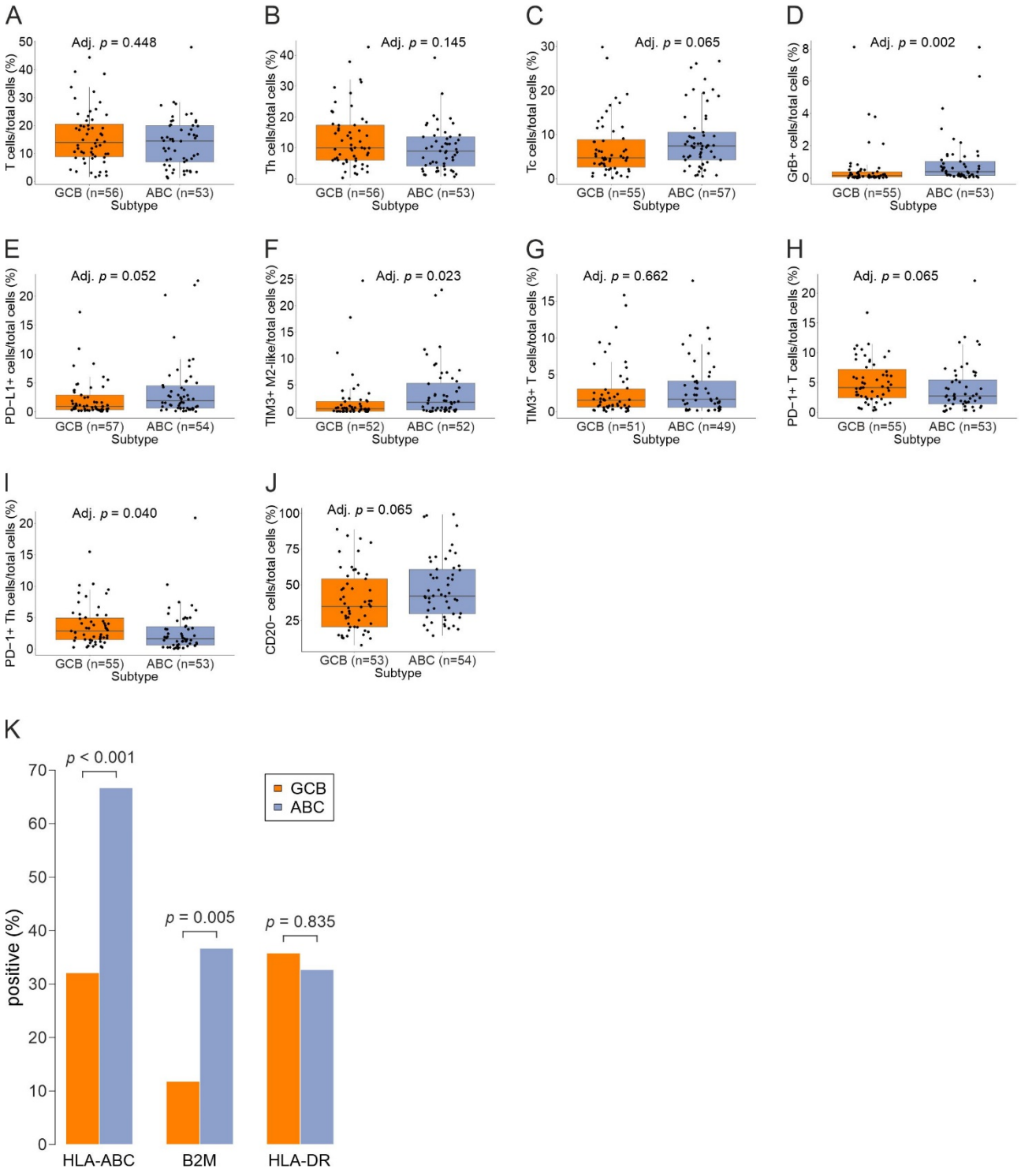

Figure S4. Proportions of immune cells in HLA and B2M positive and negative diffuse large B-cell lymphomas (DLBCLs).

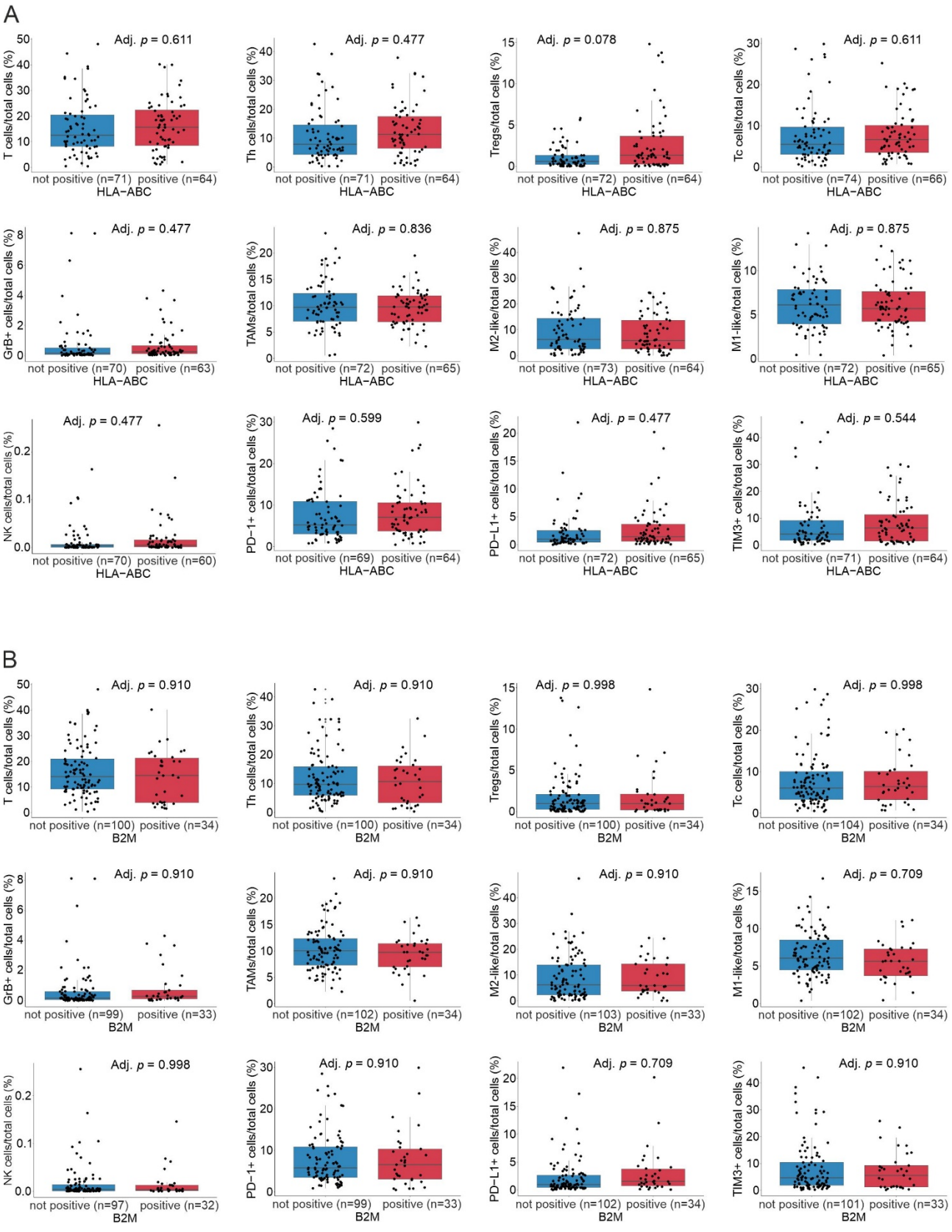

C

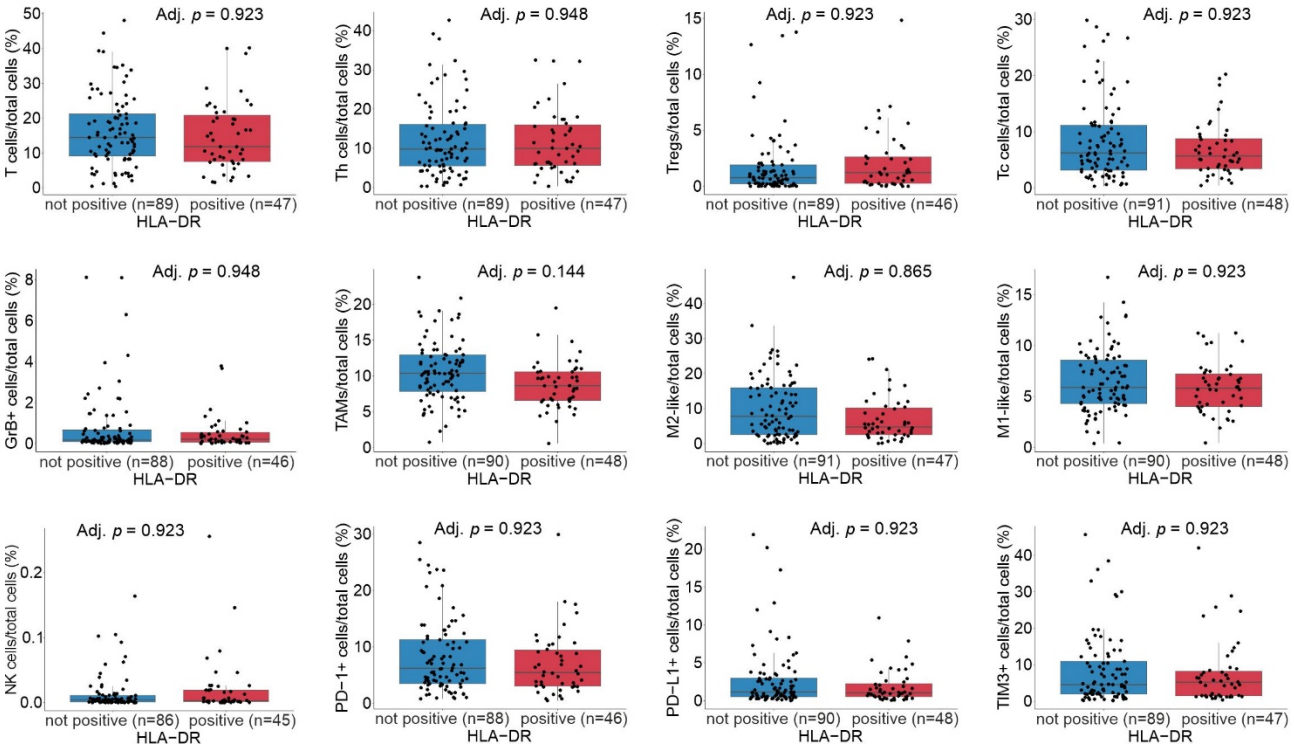
Adj. p = 0.923
T cells/total cells (%)
not positive (n=89) positive (n=47)
HLA−DR
Adj. p = 0.948
Th cells/total cells (%)
not positive (n=89) positive (n=47)
HLA−DR
Adj. p = 0.923
Tregs/total cells (%)
not positive (n=89) positive (n=46)
HLA−DR
Adj. p = 0.923
Tc cells/total cells (%)
not positive (n=91) positive (n=48)
HLA−DR
Adj. p = 0.948
GrB+ cells/total cells (%)
not positive (n=88) positive (n=46)
HLA−DR
Adj. p = 0.144
TAMs/total cells (%)
not positive (n=90) positive (n=48)
HLA−DR
Adj. p = 0.865
M2-like/total cells (%)
not positive (n=91) positive (n=47)
HLA−DR
Adj. p = 0.923
M1-like/total cells (%)
not positive (n=90) positive (n=48)
HLA−DR
Adj. p = 0.923
NK cells/total cells (%)
not positive (n=86) positive (n=45)
HLA−DR
Adj. p = 0.923
PD−1+ cells/total cells (%)
not positive (n=88) positive (n=46)
HLA−DR
Adj. p = 0.923
PD−L1+ cells/total cells (%)
not positive (n=90) positive (n=48)
HLA−DR
Adj. p = 0.923
TIM3+ cells/total cells (%)
not positive (n=89) positive (n=47)
HLA−DR

Figure S5. Differently expressed immune-related genes between testicular diffuse large B-cell lymphoma (T-DLBCL) and DLBCL, not otherwise specified (NOS).

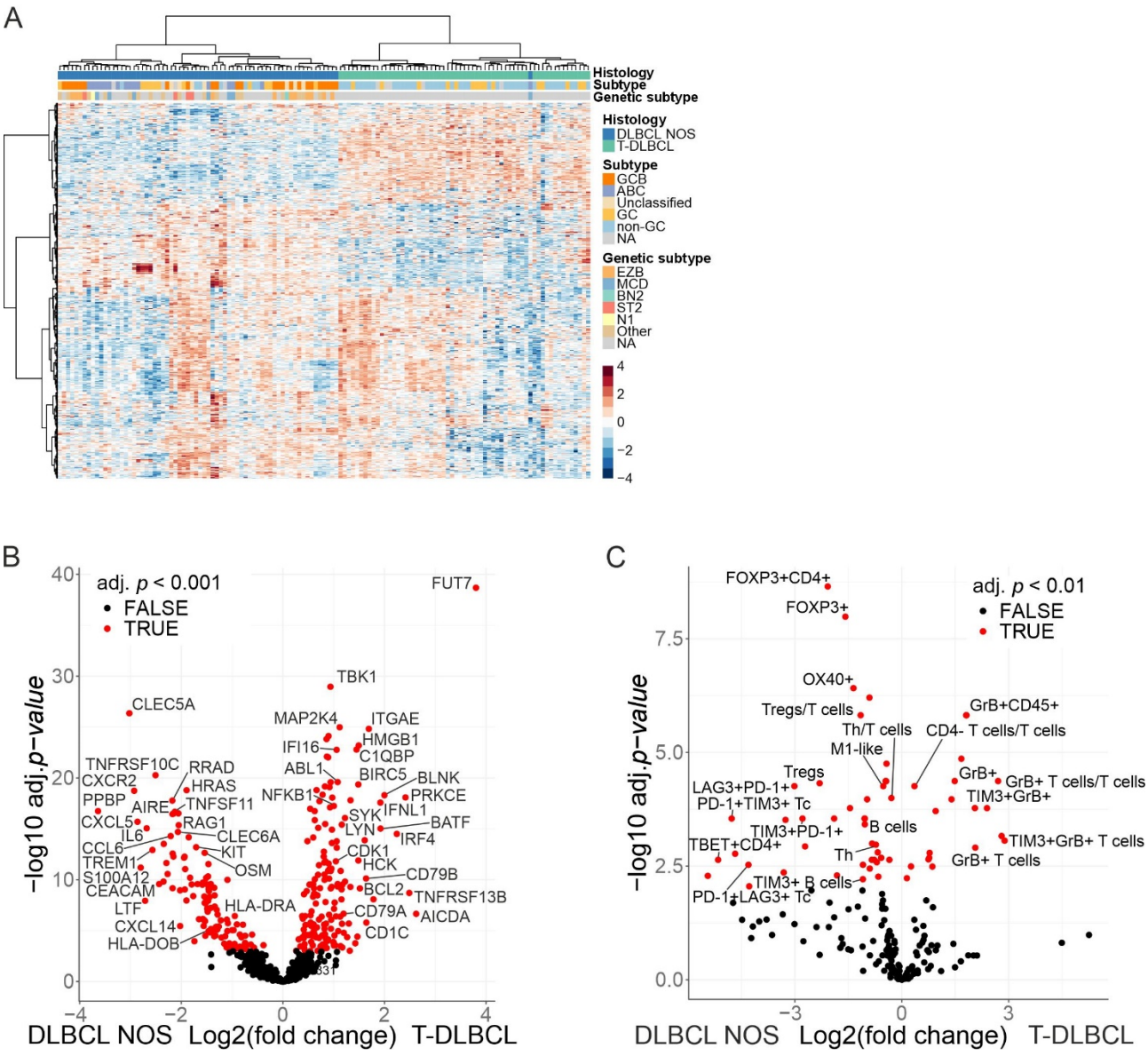

Figure S6. Differences in the constitution of the tumor microenvironment (TME) analyzed by multiplex immunohistochemistry (mIHC) between testicular diffuse large B-cell lymphoma (T-DLBCL) and DLBCL, not otherwise specified (NOS).

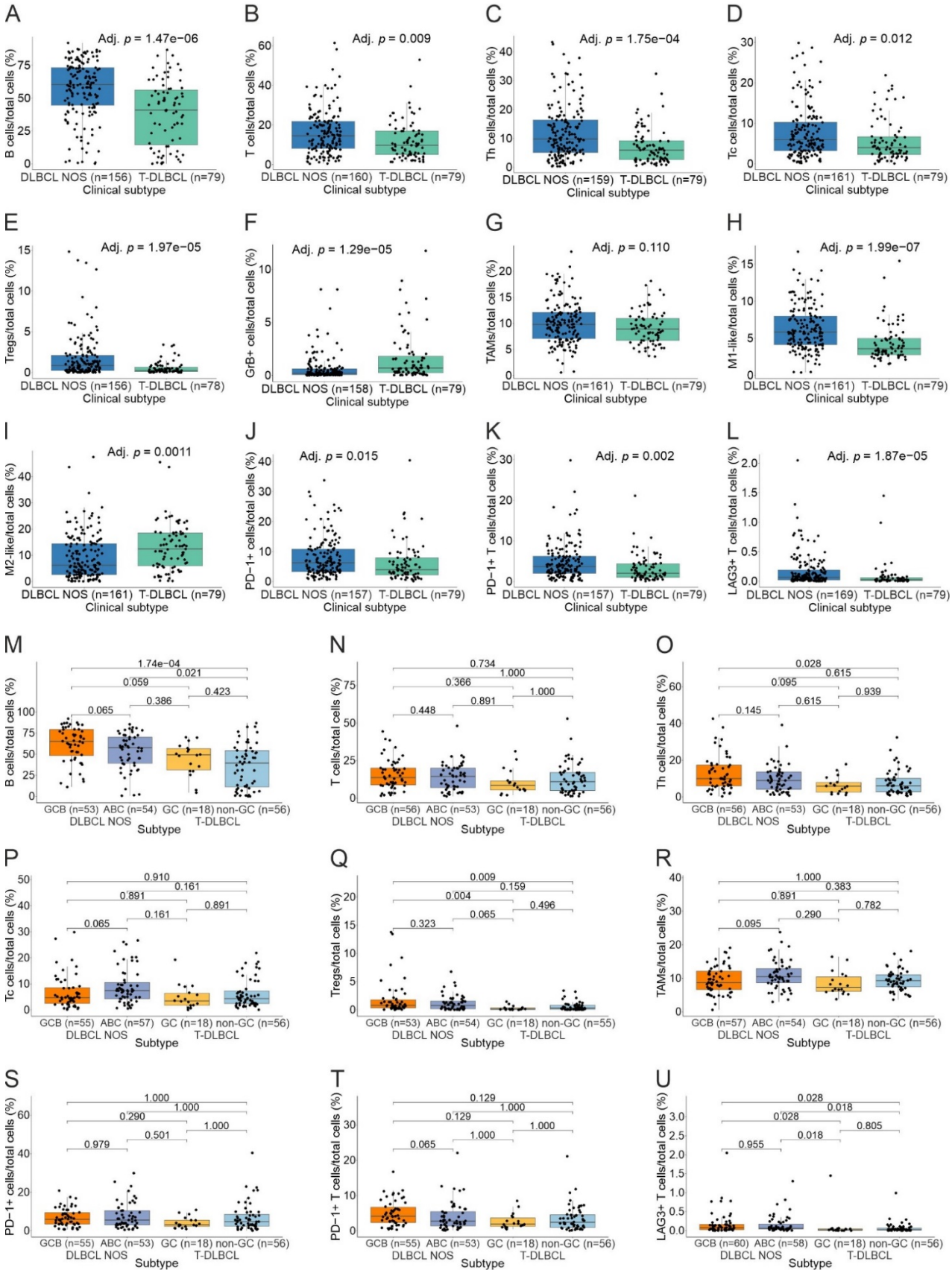

V

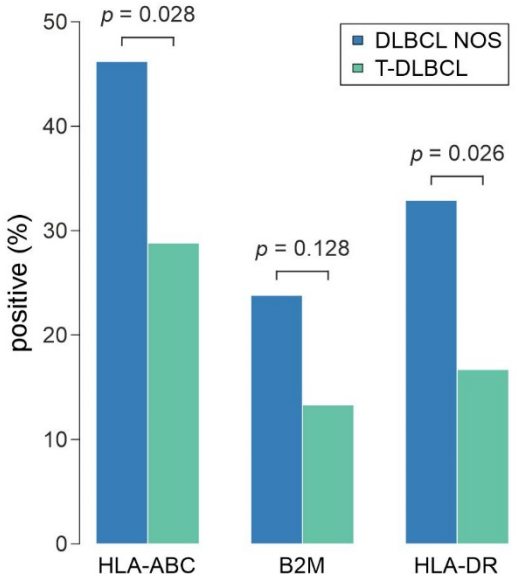
p = 0.028
p = 0.128
p = 0.026
DLBCL NOS
T-DLBCL
positive (%)
50
40
30
20
10
0
HLA-ABC
B2M
HLA-DR

Figure S7. Interactions between different immune cell subtypes in germinal center B-cell like (GCB) and activated B-cell like (ABC) diffuse large B-cell lymphoma (DLBCL) and testicular (T)-DLBCL.

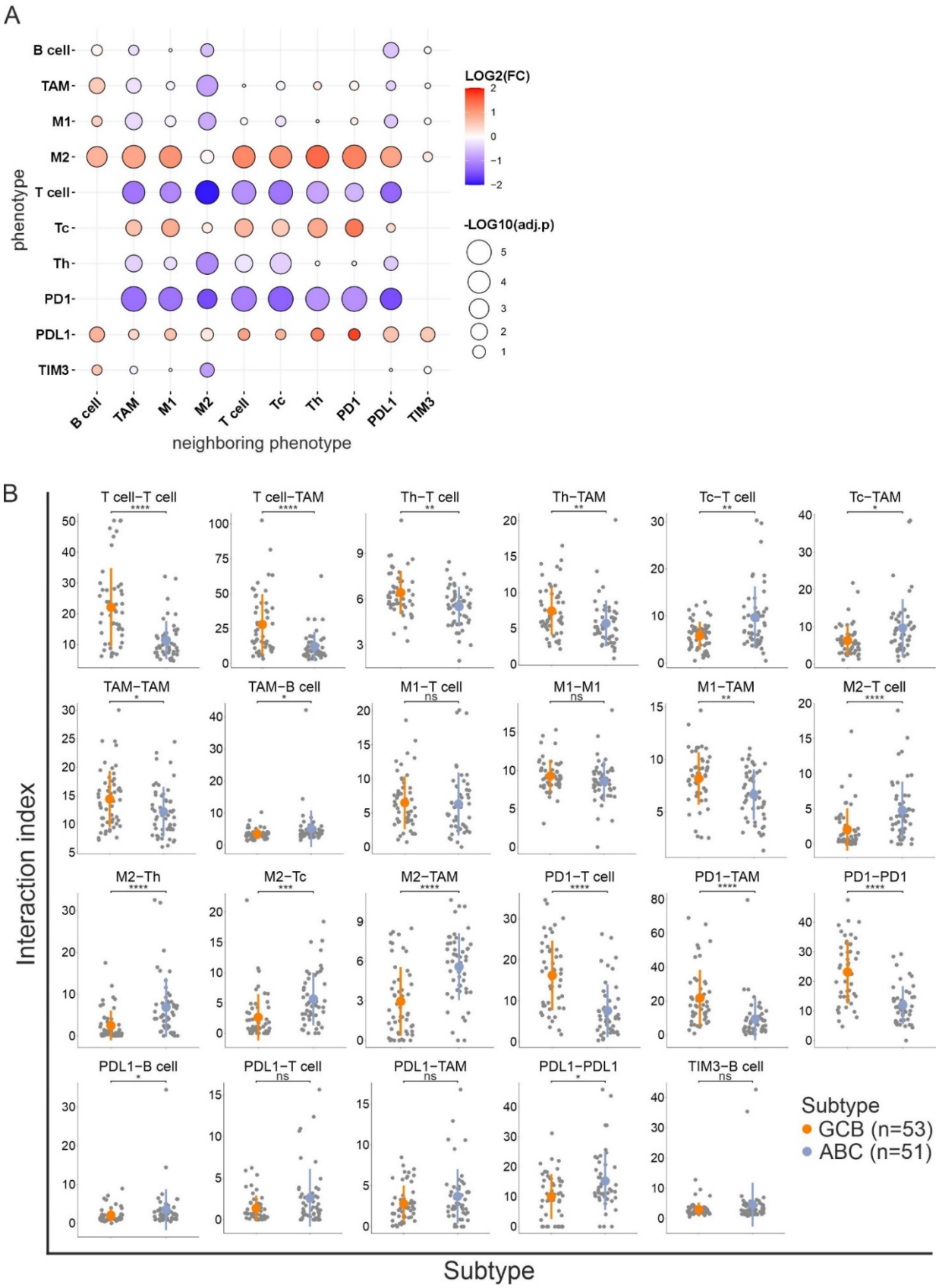

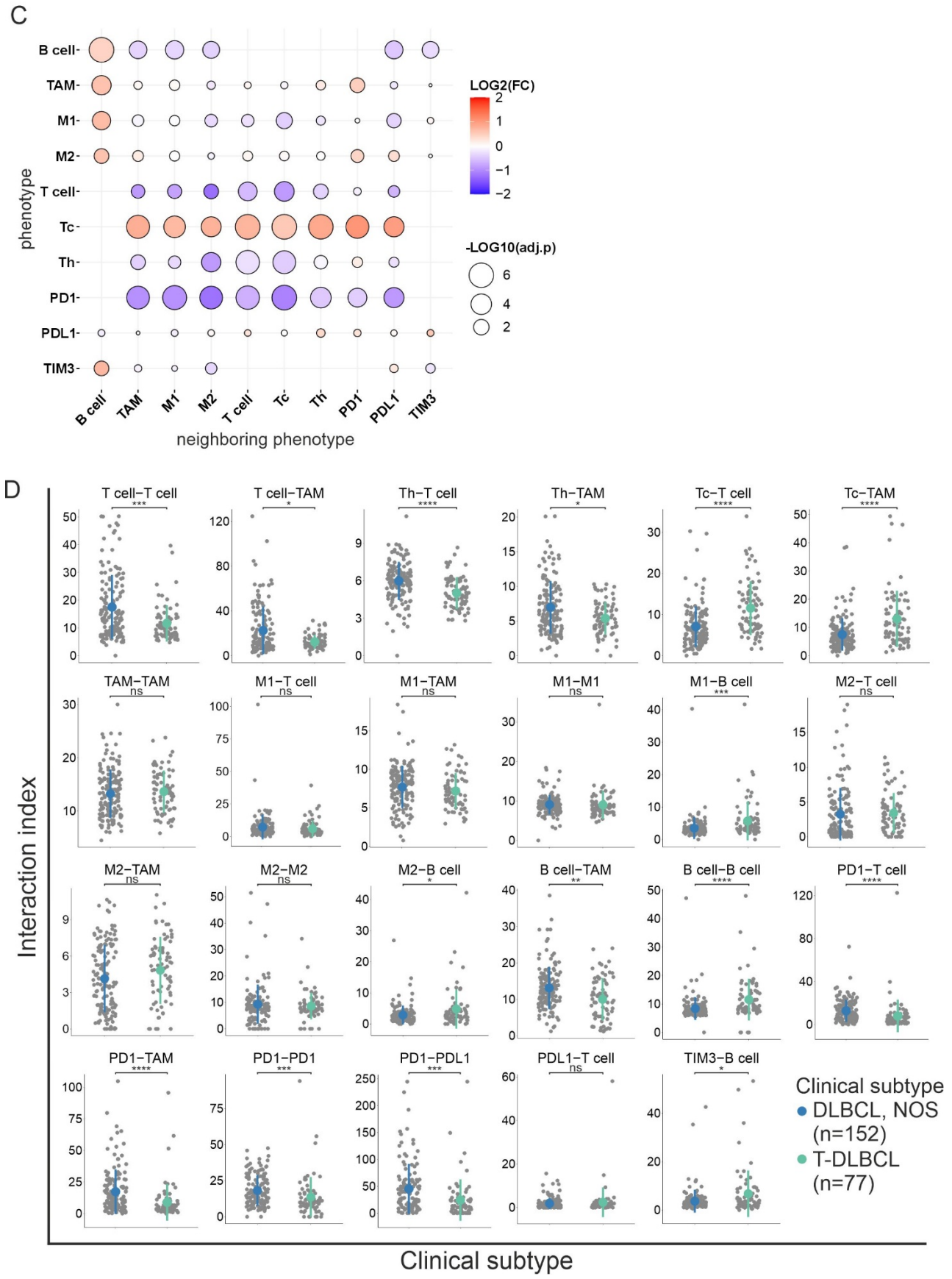
C
B cell
TAM
M1
M2
T cell
Tc
Th
PD1
PDL1
TIM3
phenotype
neighboring phenotype
LOG2(FC)
2
1
0
−1
−2
-LOG10(adj.p)
6
4
2
D
T cell−T cell
T cell−TAM
Th−T cell
Th−TAM
Tc−T cell
Tc−TAM
TAM−TAM
M1−T cell
M1−TAM
M1−M1
M1−B cell
M2−T cell
M2−TAM
M2−M2
M2−B cell
B cell−TAM
B cell−B cell
PD1−T cell
PD1−TAM
PD1−PD1
PD1−PDL1
PDL1−T cell
TIM3−B cell
Interaction index
Clinical subtype
Clinical subtype
DLBCL, NOS (n=152)
T-DLBCL (n=77)

Figure S8. Clinical impact of different immune cells and their interactions in germinal center B-cell like (GCB) and activated B-cell like (ABC) diffuse large B-cell lymphoma (DLBCL) and testicular (T)-DLBCL.

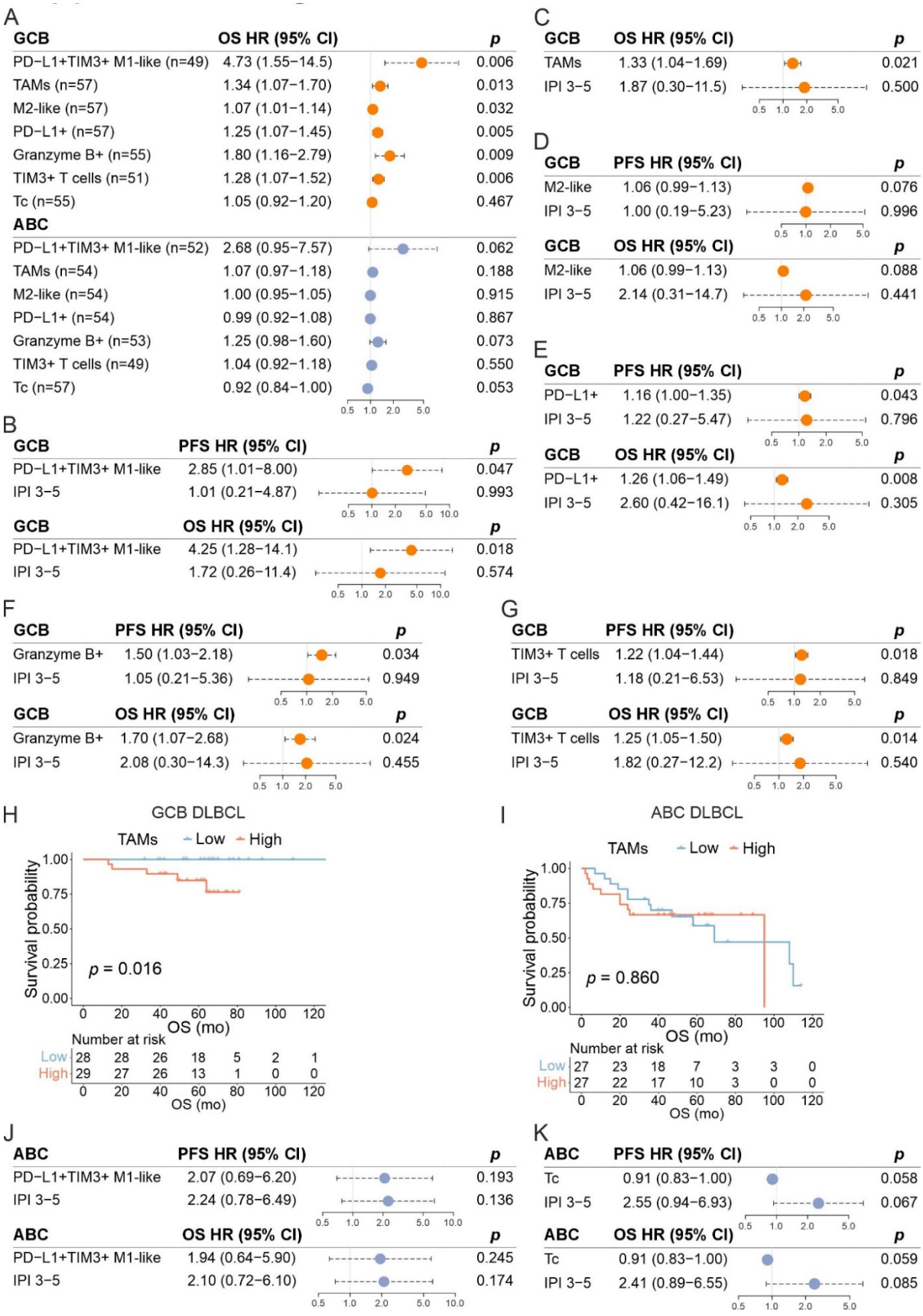

Figure S9. Clinical impact of different immune cell interactions in germinal center B-cell like (GCB) and activated B-cell like (ABC) diffuse large B-cell lymphoma (DLBCL) and testicular (T)-DLBCL.

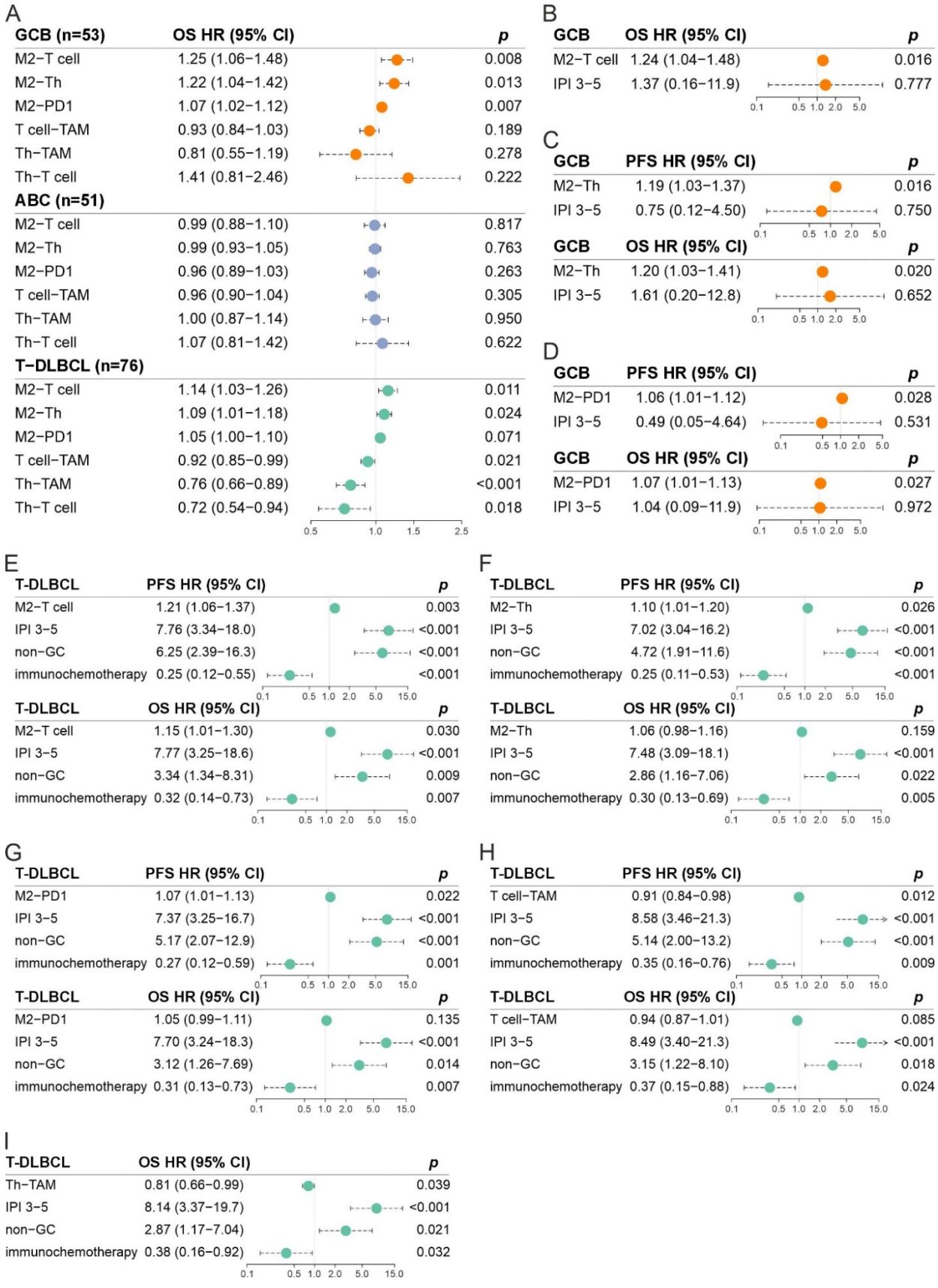

J

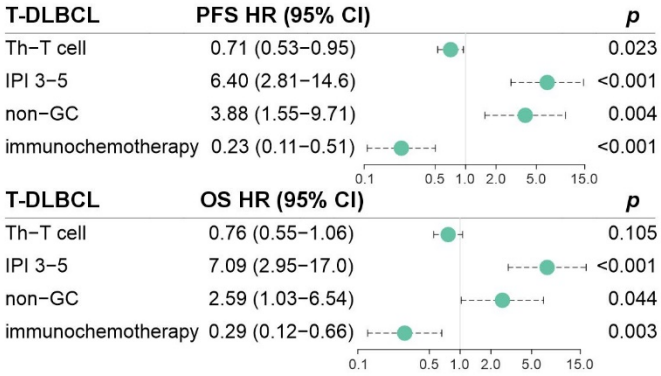
T-DLBCL
PFS HR (95% CI)
p
Th−T cell 0.71 (0.53−0.95) 0.023
IPI 3−5 6.40 (2.81−14.6) <0.001
non−GC 3.88 (1.55−9.71) 0.004
immunochemotherapy 0.23 (0.11−0.51) <0.001
0.1 0.5 1.0 2.0 5.0 15.0
T-DLBCL
OS HR (95% CI)
p
Th−T cell 0.76 (0.55−1.06) 0.105
IPI 3−5 7.09 (2.95−17.0) <0.001
non−GC 2.59 (1.03−6.54) 0.044
immunochemotherapy 0.29 (0.12−0.66) 0.003
0.1 0.5 1.0 2.0 5.0 15.0

K

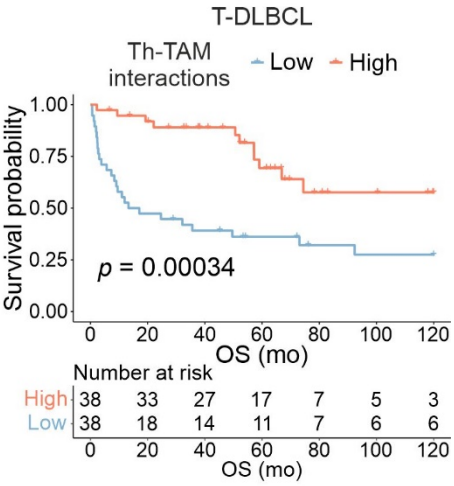
T-DLBCL
Th-TAM interactions
Low
High
Survival probability
1.00
0.75
0.50
0.25
0.00
p = 0.00034
0 20 40 60 80 100 120
OS (mo)
Number at risk
High 38 33 27 17 7 5 3
Low 38 18 14 11 7 6 6
0 20 40 60 80 100 120
OS (mo)

L

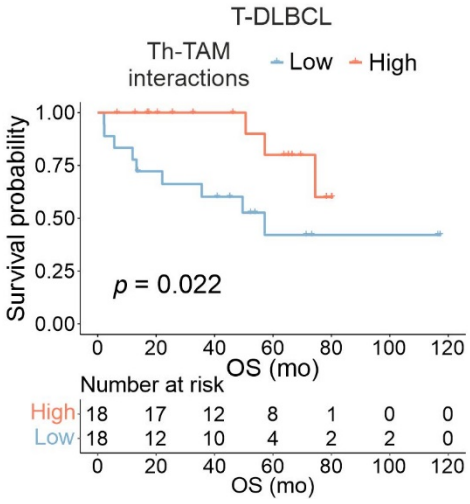
T-DLBCL
Th-TAM interactions
Low
High
Survival probability
1.00
0.75
0.50
0.25
0.00
p = 0.022
0 20 40 60 80 100 120
OS (mo)
Number at risk
High 18 17 12 8 1 0 0
Low 18 12 10 4 2 2 0
0 20 40 60 80 100 120
OS (mo)

M

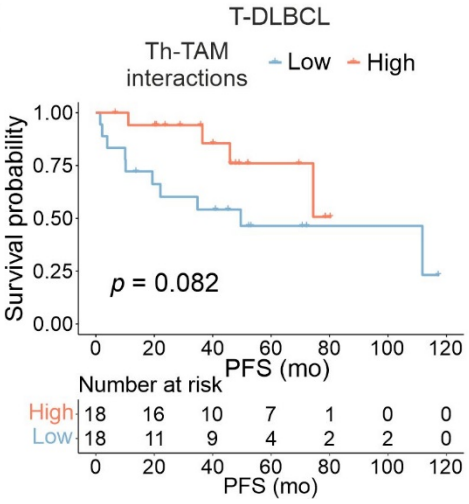
T-DLBCL
Th-TAM interactions
Low
High
Survival probability
1.00
0.75
0.50
0.25
0.00
p = 0.082
0 20 40 60 80 100 120
PFS (mo)
Number at risk
High 18 16 10 7 1 0 0
Low 18 11 9 4 2 2 0
0 20 40 60 80 100 120
PFS (mo)